6 Publikační výstupy

A. Publikace

1. Comparison of carbon-based electrodes for detection of cresols in voltammetry and HPLC with electrochemical detection
   Vosáhlová J., Sochr J., Baluchová S., Švorc L., Taylor A., Schwarzová-Pecková K., Electroanalysis 32 (**2020**), published on-line, DOI: 10.1002/elan202060103, IF 2,550 (2019)

2. Voltammetric and adsorption study of 4-nitrophenyl-triazole-labeled 2'-deoxycytidine and 7-deazaadenosine nucleosides at boron-doped diamond electrode
   Vosahlova, J., Kolacna L., Danhel A., Fisher J., Balintova J., Hocek M., Schwarzova-Peckova K., Fojta M., Journal of Electroanalytical Chemistry 821 – (**2018**) 111-120, DOI :10.1016/j.jelechem.2018.01.003, IF 3,519

3. Influence of boron content on the morphological, spectral, and electroanalytical characteristics of anodically oxidized boron-doped diamond electrodes
   Schwarzova-Peckova K., **Vosahlova J,** Barek J., Sloufova I., Pavlova E., Petrak V., Zavazalova J., Electrochimica Acta 243 (**2017**) 170-182,
   DOI: 10.1016/j.electacta2017.05.006, IF 5,478

4. Factors influencing voltammetric reduction of 5-nitroquinoline at boron-doped diamond electrodes
   Vosahlova J., Zavazalova J., Petrak V., Schwarzova-Peckova K., Monatshefte für Chemie 147 (**2016**) 21-29, DOI: 10.1007/s00706-015-1621-6, IF 1,194

5. Boron doped diamond electrodes: Effect of boron concentration on the determination of 2-aminobiphenyl
   Vosahlova J., Zavazalova J., Schwarzova-Peckova K., Chemické Listy 108 SI (**2014**) S270-273, IF 0,326

B. Příspěvky ve sbornících indexovaných ve WOS

1) Fabrication, morphology and electrochemical properties of boron doped diamond microelectrodes on tungsten supports, **J. Vosáhlová**, M. Brycht, S. Baluchová, J. Krůšek, I. Dittert, V. Mortet, A. Taylor, L. Klimša, J. Kopeček, K. Schwarzová, Proceedings of the 15th International Students Conference „Modern Analytical Chemistry“, Nesměrák K. (editor). 21. – 22. září, Praha (**2019**) Česká republika, str. 226-231, ISBN: 978-80-7444-068-7

2) Boron-Doped Diamond Electrodes: The Role of Doping Level and Surface Treatment in the Electrooxidation of m-Cresol, S. Baluchová, M. Nedvěd, **J. Vosáhlová**, A. Taylor, V. Mortet, K. Schwarzová-Pecková, XXXIX. International Conference on Modern Electrochemical Methods (Eds: T. Navrátil, M. Fojta, K. Schwarzová), 21. – 25. květen, Jetřichovice (**2019**) Česká republika, str. 9 – 13, ISBN: 978-80-905221-7-6

3) Study of Electrooxidation of Selected Phenols on Boron Doped Diamond Electrode in the Presence of Surfactants (Štúdium elektrooxidácie vybraných fenolických látok na bórom dopovanej diamantovej elektróde v prítomnosti surfaktantov), S. Baluchová, K. Procházková, **J. Vosáhlová**, and K. Schwarzová-Pecková, XXXVIII. International Conference on Modern Electrochemical Methods (Eds: T. Navrátil, M. Fojta, K. Schwarzová), 21. – 25. květen, Jetřichovice (**2018**) Česká republika, str. 11 – 14, ISBN: 978-80-905221-6-9

4) Utilization of Catalytic Hydrogen Evolution in Electrochemical Analysis of Nucleic Acids (Využití katalytického vylučování vodíku v elektrochemické analýze nukleových kyselin), **Vosahlová J.**, Schwarzová-Pecková K., Danhel A., Havan L., Fojta M., XXXVII. International Conference on Modern Electrochemical Methods (Eds: T. Navrátil, M. Fojta, K. Schwarzová), 15. – 19. květen, Jetřichovice (**2017**) Česká republika, str. 42 – 45, ISBN: 978-80-905221-5-2

5) Voltammetric Study of DNA Nucleosides Labelled by Reducible Redox Markers at Boron-Doped Diamond Electrode (Voltametrická studie DNA nukleosidů značených redukovatelnými redoxními značkami na borem dopované diamantové elektrodě), **Vosahlová J.**, Schwarzová-Pecková K., Danhel A., Havan L., Fojta M., XXXVII. International Conference on Modern Electrochemical Methods (Eds: T. Navrátil, M. Fojta, K. Schwarzová), 15. – 19. květen, Jetřichovice (**2017**) Česká republika, str. 257 – 260, ISBN: 978-80-905221-5-2

6) Electrochemical sensor based on boron doped diamond electrode for determination of phenolic compounds, Sochr J., Svorc L., Schwarzová-Pecková K., **Vosahlova J.**, Proceedings of the 13th International Students Conference „Modern Analytical Chemistry“, Nesměrák K. (editor). 21. – 22. září, Praha (**2017**) Česká republika, str. 263-267, ISBN: 978-80-7444-052-6

7) Voltammetric studies of oxidation of p-cresol at boron doped diamond electrode **Vosáhlová J.**, Barek J., Schwarzová-Pecková K., Proceedings of the 12th International Students Conference „Modern Analytical Chemistry“, Nesměrák K. (editor). 22. – 23. září, Praha (**2016**) Česká republika, str. 144-148, ISBN 978-80-7444-044-1

8) Determination of Tartazine and Allura Red at Boron Doped Diamond Electrodes (Stanovení tartrazinu a allurové červeně na borem dopovaných diamantových elektrodách), **Vosahlová J.**, Barek J., Schwarzová-Pecková K., XXXVI. International Conference on Modern Electrochemical Methods (Eds: T. Navrátil, M. Fojta, K. Schwarzová), 23. – 27. květen Jetřichovice (**2016**) Česká republika, str. 285 - 288. ISBN 978-80-905221-4-5

9) Boron-Doped Diamond Electrodes: The Effect of Surface Pretreatment on Voltammetric Signals of Phenolic Compounds, Procházková K., Baluchová S., **Vosáhlová J.**, Schwarzová-Pecková K., XXXVI. International Conference on Modern Electrochemical Methods, Jetřichovice, 23.-27. květen (**2016**) (editor: Fojta M., Navrátil T., Schwarzová K), str. 171-175, ISBN 978-80-905221-4-5

10) Utilization of boron doped diamond electrode for voltammetric study and determination of *o*-cresol (Viužitie bórom dopovanej diamantovej eletródy pre voltampérometrické štúdium a stanovenie *o*-krezolu), Sochr J., Švorc Ľ., **Vosáhlová J.**, Schwarzová-Pecková K., XXXVI. International Conference on Modern Electrochemical Methods, (Eds: Fojta M., Navrátil T., Schwarzová K), Jetřichovice, 23.-27. květen (**2016**), Česká republika, str. 206-210, ISBN 978-80-905221-4-5

11) Boron-Doped Diamond Electrodes in Electroanalysis of Reducible Organic Compounds, **Vosáhlová J.**, Zavazalova J., Petrák V., Schwarzova-Peckova K., XXXV. International Conference on Modern Electrochemical Methods, (editor: T. Navrátil, M. Fojta, K. Schwarzová) 18.–22. květen (**2015**), str. 275-279 Jetřichovice, Česká republika, ISBN: 978-80-905221-3-8

12) Electrochemical behavior of oxygen-terminated boron-doped diamond electrodes in different electrolyte media, Benesova L., Hammer P., **Vosahlova J**., Zavazalova J., Peckova K., XXXIV. International Conference on Modern Electrochemical Methods, (editor: T. Navrátil, M. Fojta, K. Schwarzová) 19.–23. květen (**2014**), str. 19-22 Jetřichovice, Česká republika, ISBN: 978-80-905221-2-1

C. Ostatní konferenční příspěvky ve sbornících

1) Reductive determination of 5-nitroquinoline with boron doped diamond electrode, **Vosáhlová J.**, Schwarzová-Pecková K.: 16th International conference on electroanalysis, 12. – 16. červen, Bath **2016** (VB). ISBN 978-186-0435-26-3

2) Factors influencing voltammetric response of m-cresol at boron doped diamond electrode, **J. Vosahlova**, K. Prochazkova, J. Barek, and K. Schwarzova-Peckova, in: Euroanalysis 2017, Stockholm, Sweden, 28. srpen - 1. září **2017**. Book of Abstracts.

3) Voltammetry study of m-cresol in the absence and presence of cationic surfactants at boron doped diamond electrode: **J. Vosáhlová**, S. Baluchová, K. Procházková, K. Schwarzová-Pecková, in: 17th International Conference on Electroanalysis (ESEAC), Rhodes, Řecko, 3. – 7. červen **2018**. Book of Abstracts, p. 162.

4) Boron doped diamond microelectrodes: Fabrication, spectral and electrochemical characterization for estimation of coverage quality, **J. Vosáhlová**, M. Brycht, J. Krůšek, I. Dittert, V. Mortet, A. Taylor, K. Schwarzová, XXV International Symposium on Bioelectrochemistry and Bioenergetics, Limerick, Irsko, 26.-30. květen **2019**, p. 241

7 Přílohy

7.1 Publikace 1

Full Paper Wiley Online Library ELECTROANALYSIS

DOI: 10.1002/elan.202060103

Comparison of Carbon-based Electrodes for Detection of Cresols in Voltammetry and HPLC with Electrochemical Detection

Jana Vosáhlová,[a] Jozef Sochr,[b] Simona Baluchová,[a] Ľubomír Švorc,[b] Andrew Taylor,[c] and Karolina Schwarzová-Pecková*[a]

Abstract: The electrochemical behavior of *o*-cresol and *p*-cresol was investigated using boron doped diamond (BDD) and sp^2 carbon-based electrodes. BDD electrodes with different boron doping levels were used to optimize conditions for detection of cresols using differential pulse and square-wave voltammetry. Comparable detection limits from 2.74 µM to 0.79 µM were achieved, using *in-situ* anodic pretreatment to prevent fouling of electrode surface. Lower detection limits for cresols and other phenolic pollutants, in the 10^{-7} M concentration range, were obtained using amperometric detection in HPLC. The proposed voltammetric and HPLC methods were utilized for determination of cresols in model river water samples.

Keywords: amperometric detection · boron-doped diamond · cresol · HPLC · voltammetry

1 Introduction

Phenol derivatives are viewed by the World Health Organization and other international health agencies as important environmental pollutants, and therefore limits for their occurrence in the environment have been set [1]. They are frequently used in industrial preparation of pesticides, dyes, plastics, detergents and drugs or are isolated by petroleum processing as minor products [2–3]. Phenols are also used as antiseptics, disinfectants or parasiticides in veterinary medicine [4]. Cresols are classified by the US Environmental Protection Agency as toxic and persistent, and as chemicals exhibiting chronic effects at a level of 12 mg L^{-1} [5–6]. The three methylphenol isomers exhibit similar physical and chemical properties. Their mixture is commonly used for wood impregnation and for production of polymers, disinfections and herbicides. Waste water from these industries and from coal conversion has a high concentration of cresols [6]. Additionally, *o*-cresol is a very specific biomarker for diagnosis of toluene exposure in clinical practice [7]. Toluene is metabolized by different ways, including conversion into hippuric and benzoic acid as main products, while all cresol isomers are secondary metabolites with the highest proportion of *ortho* isomer [8]. Production of *para* isomer is affected by tyrosine metabolism in the gut and its concentration in clinical samples is different due to food consumption. On the other hand, the amount of metabolized *meta* isomer is very low, which limits the possibilities for its determination [9]. Some studies have reported on the relationship between smoking and secretion of *o*-cresol by urine, which indicated that smoking presents a hazardous risk of intoxication of the organism [10–16].

Several instrumental analytical methods have been developed for selective and sensitive determination of phenols including cresol isomers in various matrices (*e.g.*, urine, waste water, air, and oils), such as high-performance liquid chromatography (HPLC) coupled with several detection modes including electrochemical detection [17–20], UV/VIS [7,15,21–24], diode array detection [25], fluorescence [26], and tandem mass spectrometric (MS/MS) [10,14] detection. Gas chromatography coupled with MS [9,11–12,27], flame ionization detector [8,13,16], or capillary electrophoresis [28] have also been utilized. Further, various approaches based on chemometric methods in combination with spectral methods have been established and applied successfully [4,29–31].

Possibilities of batch voltammetric methods and electrochemical biosensors for determination of cresols are presented in Table 1. In voltammetry, required selectivity and sensitivity can be reached by modification of the working electrode, most frequently a glassy carbon electrode (GCE) [2,32–33]. Modifications with cobalt(II)

[a] J. Vosáhlová, S. Baluchová, K. Schwarzová-Pecková
Charles University, Faculty of Science, Department of Analytical Chemistry, UNESCO Laboratory of Environmental Electrochemistry, Albertov 6, 128 00 Prague 2, Czech Republic
E-mail: karolina.schwarzova@natur.cuni.cz
[b] J. Sochr, Ľ. Švorc
Slovak University of Technology, Faculty of Chemical and Food Technology, Institute of Analytical Chemistry, Radlinského 9, 812 37 Bratislava, Slovak Republic
[c] A. Taylor
FZU – Institute of Physics of the Czech Academy of Sciences, Na Slovance 2, 182 21 Prague, Czech Republic

Supporting information for this article is available on the WWW under https://doi.org/10.1002/elan.202060103

Table 1. Overview of amperometric biosensors and voltammetric methods for detection of *o*-cresol and *p*-cresol.

Amperometric biosensors Compound	Electrode	Electrolyte	Method	*LDR* ($\mu mol\,L^{-1}$)	*LOD* ($\mu mol\,L^{-1}$)	Analyzed sample	Ref.
p-cresol	MWCNT/Nafion/ Tyrosine/GCE	PB (pH 7.0)	CA	1–11	0.34	n/a	[36]
p-cresol	Tyr/GCE	PB (pH 7.0)	CA	0–0.6	0.02	tap water	[37]
p-cresol	Tyr/Au_{coll}/Graphite/ Teflon	PB (pH 7.4)	CA	0.025–12	0.012	waste water	[38]
p-cresol	Tyr/AP/BDDE	PB (pH 6.5)	CA	1–200	0.1	n/a	[59]
Voltammetric methods							
p-cresol	CoPc/GCE	50 mM H_2SO_4	CV	n/a	n/a	n/a	[32]
p-cresol	MWCNT/GCE	PB (pH 7.2)	DPV	0.1–2	n/a	tap water	[2]
p-cresol	Mezo-TiO_2/GCE	AB (pH 5.0)	DPV	0.15–20	0.08	river water	[60]
o-cresol	GCE	McIlvaine buffer (pH 2.0)	LSV	20–100	42.3	n/a	[61]
o-cresol	BDDE	BR (pH 2.0)	DPV	3–100	2.63	river water	this work
p-cresol			SWV	3–100	0.61		

Abbreviations: AB – acetate buffer, AP – aminophenyl, BR – Britton-Robinson buffer, BDDE – boron-doped diamond electrode, CA – chronoamperometry, CoPc – cobalt(II) phthalocyanine, CPE – carbon paste electrode, CV – cyclic voltammetry, DPV – differential pulse voltammetry, GCE – glassy carbon electrode, LSV – linear sweep voltammetry, MWCNT – multi-walled carbon nanotubes, PB – phosphate buffer, SWV – square-wave voltammetry, Tyr – tyrosinase.

phtalocyanine and cobalt(II) octabutoxyphalocyanine have been reported for the voltammetric analyses of *o*-, *m*- and *p*-cresols [34]. Due to the passivation of the electrode surface, causing its deactivation, some reports on its modification using electroactive conducting polymers preventing such deactivation by oxidation products of cresols have been published. A relatively stable response, obtained on the same substrate electrode modified with poly(3-methylthiophene) and cobalt(II) phthalocyanine complexes, has been used to improve the stability of glassy carbon electrode for the detection of cresols and chlorophenols [35]. Specific response can be achieved by application of enzymes-based biosensors. Typically, tyrosinase immobilized on glassy carbon or graphite electrodes has been used as the biorecognition component enabling determination of cresols in various samples [36–38]. In addition, boron-doped diamond (BDD) functionalized by aminophenyl to enable covalent immobilization of tyrosinase was used for development of an amperometric biosensor for *p*-cresol determination [39].

Unmodified BDD electrodes were also used as an anode for electrochemical incineration of cresols [3,5,40–42]. The unique properties of this electrode material, such as good mechanical and chemical stability, low background current, wide potential window in the anodic region, and high resistivity to adsorption of organic compounds have been utilized in a number of voltammetric methods for determination of various oxidizable compounds [43–48] including phenolic compounds such as phenol [49], benzophenone-3 [50], nitrophenols [51], or chlorophenols [52–54]. Typically, anodically pretreated BDD films were used for this purpose as they provide high stability and the possibility of electrochemical activation of the surface [55–56]. Also, some reports exist on the advantageous properties of cathodically pretreated BDD films for detection of phenolic compounds [57–58] highlighting lower oxidation potential and faster electron transfer in comparison with anodic pretreatment.

The present work reports on a voltammetric study of the electrochemical behavior of *o*-cresol and *p*-cresol on BDD electrodes with various boron doping levels and its comparison with other common carbon-based electrode materials including carbon paste electrode (CPE), pyrolytic graphite electrode (PGE) and GCE. Additionally, a sensitive and fast voltammetric procedure for determination of cresols was developed and applied on river water samples. Furthermore, highly doped BDD electrodes were used in a "wall-jet" setup in an amperometric detection system after HPLC separation of a model mixture of phenolic pollutants, including *o*- and *p*- cresols.

2 Material and Methods

o-cresol, *p*-cresol (both of $\geq 99\,\%$ purity), hydroquinone, phenol, 4-chlorophenol, and 4-chloro-3-methylphenol were purchased from Sigma Aldrich (Prague, CZ). Stock solutions of all reagents (10 $mmol\,L^{-1}$) were prepared in deionized water and stored in a dark environment at room temperature. The pH of Britton–Robinson (BR) buffer solutions, consisting of phosphoric acid, acetic acid, boric acid (each of 0.04 $mol\,L^{-1}$) and sodium hydroxide for adjusting pH, was controlled by a digital pH-meter 3510 with a combined glass electrode (Jenway, UK). Acetonitrile (gradient grade, Merck Millipore, CZ) was used for mobile phase preparation.

All voltammetric measurements were carried out using an electrochemical analyzer, AUTOLAB PGSTAT 101, with NOVA version 1.11 software (Metrohm Autolab B. V., The Netherlands) using a three-electrode system. A platinum wire served as a counter electrode and a silver chloride electrode (Ag|AgCl, 3 mol L^{-1} KCl) was used as a reference electrode (both Elektrochemické detektory, Turnov, CZ), to which all potential values are referred to.

BDD films with various doping levels (B/C ratio in the gas phase: 500 ppm, 1000 ppm, 4000 ppm, and 8000 ppm) obtained from FZU-Institute of Physics of the Czech Academy of Sciences were placed in a laboratory-made Teflon electrode body [62] with the BDD exposed to a geometric surface area of $A = 5.72$ mm^2 (disc diameter 2.7 mm), which was employed as working electrodes in both voltammetric and amperometric measurements. Details of the fabrication procedure of BDD discs can be found in ref. [56]. The other working electrodes were: homemade PGE with square face surface area of $A = 9$ mm^2 (basal plane orientation); GCE ($A = 3.1$ mm^2, Metrohm, Switzerland) and CPE prepared from 100 µL of mineral oil (Fluka) and 250 mg of spherical microparticles of glassy carbon with diameters ranging from 0.4 to 12 µm (Alfa Aesar, USA) packed in the Teflon electrode body with an active surface of $A = 3.1$ mm^2. Pretreatment and activation of electrode surfaces were carried out as follows: polished BDD (p-BDD) electrode – pretreated by polishing for 3 min using suspension of alumina (particle size of *ca* 0.5 µm, Elektrochemické detektory, Turnov, CZ) in deionized water, alumina residues were subsequently removed from the p-BDD surface by sonication in methanol and deionized water. Prior to each scan, activation was carried out by polishing using an alumina suspension for 30 s; O-BDD – pretreatment performed daily at the beginning of series of measurements by applying +2.4 V for 5 min in a stirred solution of 0.5 mol L^{-1} H_2SO_4. Anodic activation at +2.4 V for 1 min directly in a measured solution was also applied between individual scans in measurements of scan rate dependence by cyclic voltammetry and in an optimized differential pulse voltammetry (DPV) procedure. GCE – polishing (for 30 s) prior to each scan using alumina suspension followed by thorough washing with deionized water. PGE – surface left to dry at air after each scan and renewed using adhesive tape.

Optimized operation parameters for DPV and SWV were used, if not stated otherwise: pulse height of +100 mV, pulse width of 50 ms, interval time of 200 ms and a scan rate of 20 mV s^{-1} for DPV and an amplitude of 70 mV and frequency of 25 Hz for SWV.

The HPLC system consisted of an ECB2004 gradient box with degasser, an ECP2010 analytical pump, an ECD2800 UV-VIS detector (all ECOM, Prague, CZ), and amperometric detector ADLC 2 (Laboratorní přístroje, CZ) connected in series. Chromatographic separation was achieved on an end-capped reversed phase column Purospher RP-18, 5 µm, 125 mm × 4 mm I.D. directly attached to a guard column Purospher RP-18, 5 µm, 4 mm × 4 mm (both Merck, Germany) under isocratic conditions. The mobile phase consisted of 0.04 mol L^{-1} BR buffer (pH 2.0) and acetonitrile mixed in a ratio of 60/40 (*v/v*; final concentration of each acid of BR buffer was 0.024 mol L^{-1}). The injection volume was 20 µL and measurements were performed with a constant flow rate of 1 mL min^{-1}. UV detection was performed at a wavelength of 280 nm. Amperometric detection used the same electrode set as for voltammetric experiments, in which the working BDD electrode with a B/C of 8000 ppm was adjusted against the outlet capillary in a "wall-jet" arrangement and an optimized detection potential of +1.6 V was applied. An overflow wall-jet detection cell [63] was used keeping the capillary outlet (diameter 0.15 mm) – electrode surface distance at 0.5 mm. The HPLC system was controlled by Clarity 7.3 software (DataApex, CZ).

Water samples for analysis, obtained from the local Vltava river, were initially filtered through a nylon syringe filter (0.45 µm, Fischer Scientific, CZ), subsequently diluted ten times with BR buffer (pH 2.0) and then injected directly into the chromatographic system. Furthermore, spiked water samples were analyzed and the standard addition method was used to determine concentrations of selected phenols.

Voltammetric curves were smoothed using a Savitzky-Golay filter (level 4) and each signal was baseline corrected. Data evaluation was processed by Origin 8. *LOD* values were calculated as three times the standard deviation of the peak current for the lowest measurable concentration divided by the slope of calibration curve ($n = 10$). For HPLC measurements, concentration dependences were constructed from the average of three replicate measurements for each calibration solution of the selected phenols and evaluated by the linear least squares regression method. *LOD* values were calculated as a threefold and *LOQ* values as a tenfold of the average background noise, divided by the slope of the corresponding linear concentration dependence *k*.

3 Results and Discussion

3.1 Cyclic Voltammetry of *o*- and *p*-cresol on Carbon-based Electrode Materials

The electrochemical behavior of *o*-cresol and *p*-cresol was studied using CV on BDD electrodes with O-terminated and polished surfaces, and further on pyrolytic graphite, glassy carbon and carbon paste electrode. Cathodically pretreated (H-terminated) BDD was excluded from the study after preliminary experiments. While the signal intensities resembled p-BDD, it was quickly recognized that fouling of the BDD surface, caused by reaction (by) products of oxidation of cresols, can only be overcome by polishing or anodic pretreatments, leading to conversion of H-terminated BDD to O-BDD. Therefore, the application of a cathodic pretreatment, after these successful activation approaches following each scan, has been

evaluated as a redundant step causing prolongation of the operation procedure with no added benefit regarding the obtained sensitivity. Figure 1 presents the 1st, 2nd and 10th cycle recorded in BR buffer (pH 2.0) on these electrodes. The reaction mechanism is summarized in Scheme 1 presenting also the variety of mesomeric forms of formed species; typical anodic and cathodic signals at the voltammetric curves are described in Figure 1A and 1E for *o*-cresol on p-BDD and GCE, respectively. Both cresols (*o*-cresol **1**, *p*-cresol **9**) were found to be oxidized by $1e^-/1H^+$ exchange at the potential of +1.1 V–+1.2 V on BDD electrodes and lower potential of *ca* +0.9 V–+1.0 V on the other electrodes (peak 1_a) forming methylphenoxy-type –O• radical (**2**, **10**), a typical primary product of oxidation of phenolic compounds [32,64–66]. This reaction is easily observable on all tested electrode materials. The positive shift of the peak 1_a is a consequence of hindered electron transfer on the heterogeneous surface of BDD [67–69]. This reaction may be followed by another oxidation process at the potential of +1.3 V (peak 2_a) leading to carbocationic species (methylphenoxy cation (**3**, **11**)), it is most pronounced on p-BDD electrodes with an extended potential window in comparison with the other sp^2 carbon-based electrodes and faster electron transfer kinetics in comparison with O-BDD surfaces [67,70]. These methylphenoxy cations (**3**, **11**) possess the same variety of mesomeric forms as methylphenoxy-type –O• radicals (**2**, **10**). Further chemical reaction steps, reaction with water, leads to formation of methylhydroquinone(s) (**5**, **6**, **12**), which are readily oxidized in $2e^-/2H^+$ reaction to methylquinone(s) (**7**, **8**, **13**). In a parallel reaction of radicals (**2**, **10**), eventually cationic species (3,11), dimeric and polymeric species are formed [64,71,72] causing passivation of the electrode surface, as proved by a decrease of the 1_a peak with increasing number of scans (Figure 2). Similarly, the reaction of methylhydroquinone(s) (**5**, **6**, **12**) to methylquinone(s) (**7**, **8**, **13**) proceeds through radical intermediates, which are stabilized by mutual reactions resulting in formation of polymeric species [66]. The species can possess hydroxyl, quinonic, or hydroquinone moieties and thus can be seen in further scans, as commented below. In the reverse cathodic scan, reduction peaks 3_c and 4_c are observed at *ca* +0.65 V–+0.45 V, representing reduction of the simplest cresol oxidation product(s) – reduction of methylquinone(s) (**7**, **8**, **13**) to corresponding methylhydroquinone(s) (**5**, **6**, **12**). In the second cycle, two new oxidation peaks appear at +0.55 V (peak 4_a) and +0.65 V (peak 3_a, at Figure 1A only insinuated). They correspond to $2e^-/2H^+$ oxidation of methylhydroquinone (s) (**5**, **6**, **12**) to corresponding quinones (**7**, **8**, **13**).

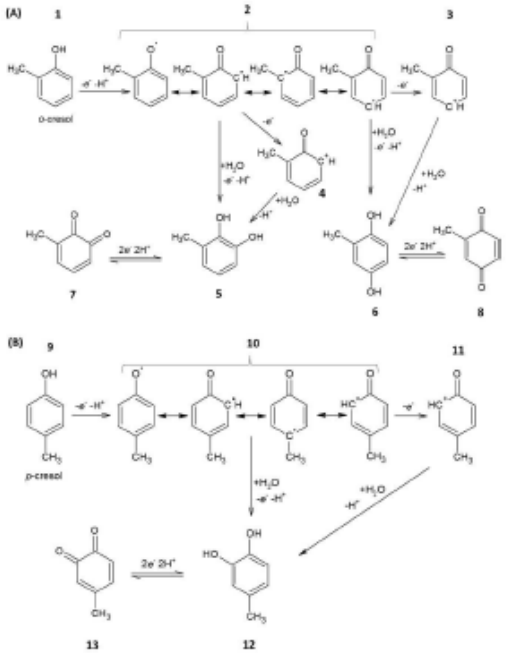

Scheme 1. Reaction mechanism of electrochemical oxidation of *o*- and *p*-cresol.

This general reaction mechanism is strongly influenced by the type of carbonaceous material and structure of the cresol. When comparing recorded CVs of *o*- and *p*-cresol, a noticeable difference is that the signals of redox pairs (peak $3_a/3_c$ and $4_a/4_c$) are absent or insinuated for the latter isomer, but well recognizable for the former. Obviously, reaction products of *p*-cresol (besides methylhydroquinone) (**5**, **6**, **12**) and methylquinones (**7**, **8**, **13** also species produced by parallel reaction) possess lower proclivity to adsorption on the electrode surface. This compound has a lower number of mesomeric forms of reaction intermediates (methylphenoxy-type –O• radicals and cations) than *o*-cresol (Scheme 1) leading to simple hydroquinones/quinones not adsorbing on electrode surface. *o*-cresol possesses a higher number of mesomeric forms and thus products arising from their crosslinking reactions capable of adsorption on all electrode materials. The only electrode exhibiting clear signals of peak pairs $3_a/3_c$ and $4_a/4_c$ also for *p*-cresol is CPE due to the additional interaction of the hydrophobic reaction products with the binder.

Importantly, the first anodic signal 1_a decreases with consecutive cycling, as seen in Figure 2 comparing the relative decrease of the 1_a signal within 10 cycles. This fouling of the electrode surface is of different significance when comparing particular electrode materials. For both compounds, the O-BDD surface is the most resistive towards blocking by reaction products (ca 95 % in the 2nd scan, and 75 % in the 10th scan of the original *o*-cresol signal obtained in the 1st scan), together with CPE (*ca* 50 % decrease within ten scans). p-BDD surface is only resistive to fouling by *p*-cresol reaction products, but is almost completely blocked by *o*-cresol, confirming again

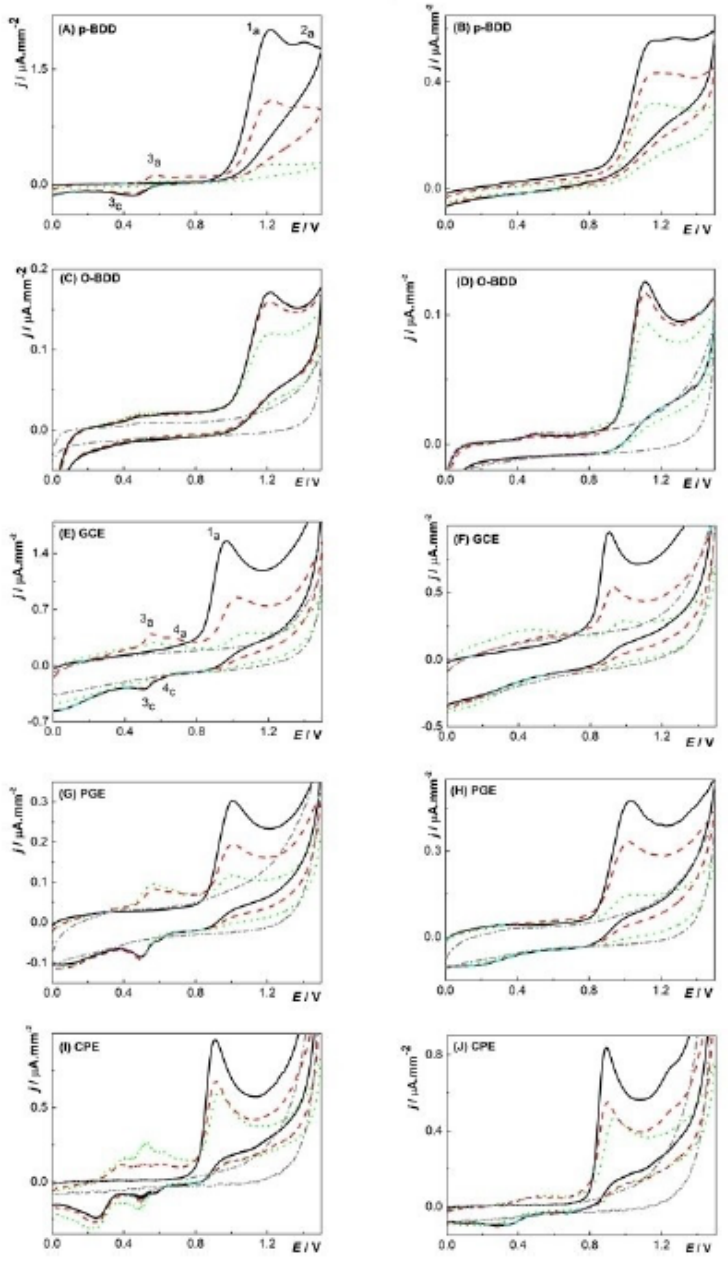

Fig. 1. Cyclic voltammograms of 0.1 mmol L^{-1} *o*-cresol (left column) and *p*-cresol (right column) in BR buffer (pH 2.0) for the 1st (full line), 2nd (dashed line), and 10th (dotted line) scan on (A) and (B) p-BDD electrode, (C) and (D) O-BDD electrode, (E) and (F) GCE, (G) and (H) PGE, and (I) and (J) CPE. Recorded from 0 V to + 1.5 V at a scan rate of 0.1 V s^{-1}.

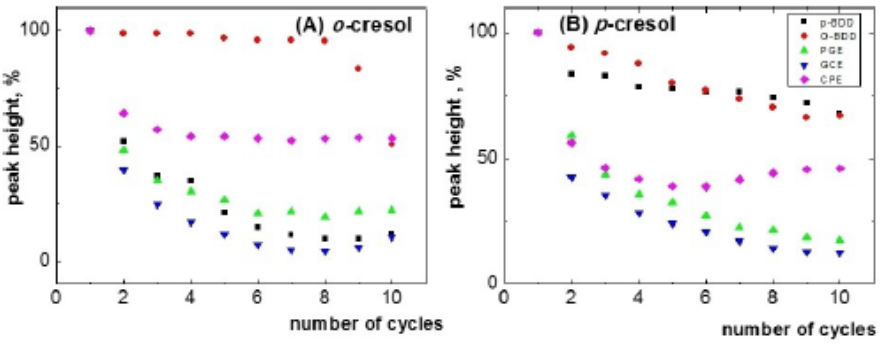

Fig. 2. Relative decrease of the height of the first anodic signals for 0.1 mmol L^{-1} (A) *o*-cresol and (B) *p*-cresol during ten consecutive CV scans recorded from 0 V to +1.5 V. Measured in BR buffer (pH 2.0) at a scan rate of 0.1 Vs^{-1} on (■) p-BDD electrode, (●) O-BDD electrode, (▼) GCE, (▲) PGE and (♦) CPE.

the impact of their different structure on proclivity to adsorption as mentioned above.

Further experiments were performed only with BDD electrodes to achieve an operation protocol for detection of cresols with *tn-sttu* regeneration of the electrode surface for passivation prevention. The effect of electrochemical activation using highly positive (+2.4 V) and negative (−2.4 V) potentials with intensive stirring between the individual measurements for studied cresols was investigated. Repeatable peak heights were obtained in the case of anodic activation for 1 min. At highly positive potentials, in the region of water decomposition, reactive hydroxyl radicals are generated, which oxidize organic compounds into smaller molecules and finally into CO_2 and H_2O. Thus, any polymer film is removed from the electrode surface, as presented also for other phenolic compounds at BDD electrodes [33,50,73–75]. This regeneration resulted in relative standard deviation (*RSD*) values of signal heights 8.6 % (DPV) and 2.6 % (SWV) for *o*-cresol, and 15.6 % (DPV) and 12.6 % (SWV) for *p*-cresol. Despite the significant passivation of the BDD electrode surface during the cresol sensing, these values are relatively low. Without regeneration steps between each measurement, these values were higher than 30 %, thus providing very poor repeatability.

3.2 Voltammetric Behaviour of *o*- and *p*-cresol on O-terminated BDD Electrode

3.2.1 Effect of pH

O-terminated BDD electrodes, offering the possibility of *tn-sttu* activation, were further used to address the effects of supporting electrolyte, boron doping level and pulse method on voltammograms of *o*- and *p*-cresol and for their application for detection of these compounds. pH dependences of peak potentials and peak currents were studied using DPV on O-BDD electrodes. Figure 3 clearly indicates that peak potential values for both cresols are pH-independent up to a pH value of *ca* 10 and then a

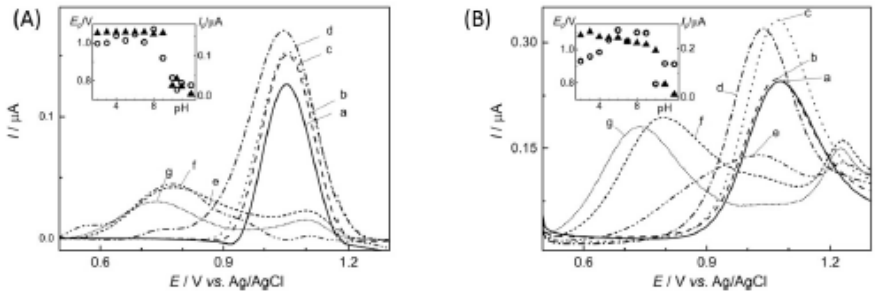

Fig. 3. DP voltammograms of (A) 10 µmol L^{-1} *o*-cresol and (B) 10 µmol L^{-1} *p*-cresol using 8000 ppm BDD electrodes for the following pH values of BR buffer: a.) 2.0, b.) 4.0, c.) 6.0, d.) 8.0, e.) 10.0, f.) 11.0, g.) 12.0. In insets, the pH dependencies of oxidation peak potential (▲) and the peak current value (○) are shown.

drop of about 0.25 V to less positive values with increasing pH is observed. pH 10 corresponds to pK_a values of *o*-cresol and *p*-cresol; the same value of 10.26 (ref. [76]) or similar pK_a values of 10.28 and 10.19 (ref. [77]) were reported in the literature. Easier oxidation of the dissociated phenolate anion at $pH > pK_a$ is associated with the availability of an electron directly in the electron pair of an oxygen atom and negative charge of the phenolate species being attracted to the positively charged electrode. Interestingly, two types of pH-dependence are being reported for peak potentials E_p of simple phenolic compounds. Most frequently, the linear dependence of E_p *vs.* pH spanning over the pH corresponding to pK_a with a slope of about 59 mV per pH unit is attributed to one-electron and one-proton process, *e.g.*, for phenol [64] on a GCE, benzophenone-3 on an anodically oxidized BDD electrode [50], and 2,4-dichlorophenol on both as-received and anodically-oxidized BDD electrodes [75]. On the other hand, pH-independency at pH values smaller than pK_a was reported, *e.g.* for 4-chloro-3-methylphenol on anodically oxidized BDD electrode [78]. Apparently, both the structure of the phenolic compound and surface condition influences the oxidation process.

The current response of studied cresols is also changing at the pH value around pK_a. Voltammetric peaks of dissociated *o*- and *p*-cresol in alkaline medium have lower heights and deformed shapes in comparison with acidic and neutral pH. Therefore, a BR buffer (pH 2.0) was chosen as the supporting electrolyte for further experiments.

3.2.2 Effect of Boron Doping Level and Analytical Performance Assessment

Boron doping level affects the electron transfer rate between the electrode surface and an analyte, and thus changes the sensitivity of determination, especially when using pulse techniques. In our previous studies, we have reported on the negative shift of peak potential and increase of peak current with increasing boron-doping level for DP voltammetric determination of benzophenone-3 [50], 4-chloro-3-methylphenol [78], or 2-aminobiphenyl [56] with the most pronounced differences between the semi-conductive BDD films (500 ppm and 1000 ppm) and films with metallic type conductivity (2000 ppm –8000 ppm). Also, other authors reported an increase in peak currents, *e.g.*, for oxidation of uric acid [79] or reduction of nitrofurantoin [80]. Figure 4 shows the DP voltammetric curves obtained for *o*-cresol and *p*-cresol for the set of 500 ppm–8000 ppm electrodes with I_p and E_p *vs.* boron-doping level dependencies in insets. Their values confirm the trends described above. Accordingly, the slopes of calibration dependences (sensitivity) are increasing with boron-doping level (see Table 2). The linear concentration range is from 3.0 to 100 $\mu mol\,L^{-1}$ for all working electrodes and DPV and SWV techniques. The *LOD*s listed in Table 2 are in the range from 2.74 $\mu mol\,L^{-1}$ to 0.79 $\mu mol\,L^{-1}$, irrespective of the compounds and method used. For their calculation, values of slope and standard deviations s_r of peak heights of the lowest measurable concentration were used (see section 2. Material and Methods). The lower slope values for semi-conductive 500 ppm and 1000 ppm BDD films are compensated by lower s_r values. They result from partial "inactivity" of the heterogenous BDD surface toward charge transfer reactions, leading to higher consistence of electrochemical characteristics including electrode response towards oxidation of cresols. As a result, the studied BDD films show comparable properties from an analytical point of view for detection of cresols.

For further applications, BDD film with 8000 ppm B/C content was used. It is the most sensitive among the other films for cresols determination according to the slope value (Table 2), which has the advantage of simplifying evaluation of signals obtained for low concentrations of studied phenols. Otherwise, comparable results regarding detection limits are expected as explained above.

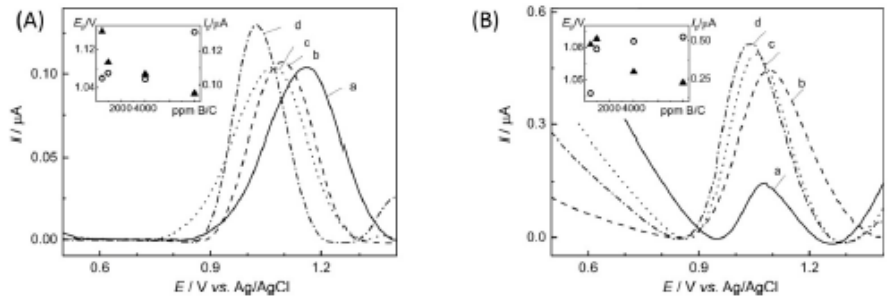

Fig. 4. DP voltammograms of (A) 50 $\mu mol\,L^{-1}$ *o*-cresol and (B) 50 $\mu mol\,L^{-1}$ *p*-cresol recorded on BDD electrodes deposited using B/C ratio (ppm) (a) 500, (b) 1000, (c) 4000, and (d) 8000. The insets show dependencies of peak potential (▲) and peak current (○) on B/C ratio used during the BDD film deposition process.

Table 2. Parameters and limits of detection obtained from calibration dependences for *o*-cresol and *p*-cresol for linear dynamic range of 3–100 μmol L^{-1}. Measured by DPV and SWV using BDD electrodes with different B/C ratio in BR buffer (pH 2.0).

B/C ratio (ppm)	Isomer	Regression equation (I_p in μA, c in mmol L^{-1})	R	*LOD* (μmol L^{-1})
Differential pulse voltammetry				
500	*o*-cresol	$I_p = 4.94\ c - 0.024$	0.9945	1.05
	p-cresol	$I_p = 4.37\ c + 0.105$	0.9991	1.25
1000	*o*-cresol	$I_p = 6.54\ c - 0.016$	0.9954	1.16
	p-cresol	$I_p = 6.23\ c + 0.068$	0.9998	1.37
4000	*o*-cresol	$I_p = 13.16\ c + 0.074$	0.9846	2.67
	p-cresol	$I_p = 10.84\ c + 0.014$	0.9870	0.74
8000	*o*-cresol	$I_p = 14.75\ c + 0.010$	0.9897	2.63
	p-cresol	$I_p = 10.66\ c + 0.084$	0.9970	0.61
Square-wave voltammetry				
500	*o*-cresol	$I_p = 6.15\ c - 0.022$	0.9912	1.01
	p-cresol	$I_p = 5.13\ c + 0.004$	0.9938	0.69
1000	*o*-cresol	$I_p = 9.48\ c - 0.024$	0.9957	1.07
	p-cresol	$I_p = 7.73\ c - 0.003$	0.9981	1.06
4000	*o*-cresol	$I_p = 13.80\ c + 0.017$	0.9857	2.58
	p-cresol	$I_p = 9.62\ c - 0.019$	0.9899	1.30
8000	*o*-cresol	$I_p = 15.05\ c - 0.053$	0.9895	2.97
	p-cresol	$I_p = 11.09\ c - 0.019$	0.9872	1.52

3.3 HPLC with Amperometric Detection on O-terminated BDD Electrodes

Prior HPLC measurements in which mixed aqueous-organic mobile phase was used (BR buffer (pH 2.0) and acetonitrile (60:40, *v/v*)), voltammetric experiments were carried out with O-BDD film (8000 ppm B/C) to assess the effect of different content of acetonitrile (varying from 1 % to 40 %) in supporting electrolyte on the electrochemical responses of studied cresols (see Figure S1 in Supplementary material). In case of both cresols, peak potential shifted to more positive values with increased acetonitrile content (a shift by 240 mV for *o*-cresol and by 160 mV for *p*-cresol was observed in the presence of 40 % v/v acetonitrile) whilst recorded peak currents were not significantly affected by the addition of organic solvent. During five consecutive scans without applying any activation procedure, substantial signal drop for both cresols of about 45 %–60 % was observed for the acetonitrile content 0–20 %. For higher content, the fouling was slightly suppressed, the signal drop was about 15 %–30 %, *t.e.* smaller but still significant. Nevertheless, this fouling was completely avoided under liquid flow conditions in HPLC measurements as further described below.

An O-terminated BDD electrode, with B/C of 8000 ppm, was then inserted into a wall-jet amperometric flow cell-electrochemical detector (ED) arranged after the UV-VIS detector (UVD) of the HPLC system. A model mixture, including commonly occurring phenolic compounds in river and waste water, such as phenol, hydroquinone, *o*- and *p*-isomers of cresol, 4-chlorophenol, and 4-chloro-3-methylphenol, was separated on a reversed C-18 phase under isocratic conditions. The separation was completed in 7.0 min (Figure 5A) with the following elution order of analytes: 1) hydroquinone, 2) phenol, 3) *p*-cresol, 4) *o*-cresol, 5) 4-chlorophenol, and 6) 4-chloro-3-methylphenol. Retention times and retention factors are listed in Table 3. Moreover, peak resolutions (R) for both detectors were calculated and obtained values are presented: $R_{1,2}$ 13.33, $R_{2,3}$ 8.80, $R_{3,4}$ 2.22, $R_{4,5}$ 4.72, and $R_{5,6}$ 12.65 for UVD, and $R_{1,2}$ 8.64, $R_{2,3}$ 6.14, $R_{3,4}$ 2.32, $R_{4,5}$ 3.58, and $R_{5,6}$ 10.37 for ED. Evidently, all values are higher

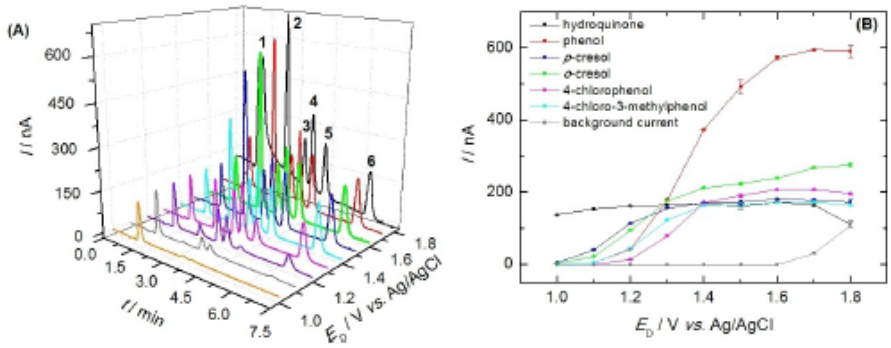

Fig. 5. (A) Chromatograms of the mixture containing selected phenols (each of $c = 10$ μmol L^{-1}) recorded at different values of applied detection potential E_D, analytes eluted as follows: (1) hydroquinone, (2) phenol, (3) *p*-cresol, (4) *o*-cresol, (5) 4-chlorophenol, and (6) 4-chloro-3-methylphenol. (B) Hydrodynamic voltammograms of selected phenols (each of $c = 10$ μmol L^{-1}) and dependence of the background current on the applied detection potential E_D on the O-BDD electrode with B/C of 8000 ppm. Error bars represent standard deviations ($n = 4$). Measured by HPLC with a wall-jet detection cell, column Purospher RP-18, 5 μm, 125 mm × 4 mm, mobile phase BR buffer (pH 2.0) and acetonitrile (60:40, v/v), isocratic elution, injection volume of 20 μL, flow rate of 1 mL min^{-1}.

Table 3. Retention times and factors and *LOD* and *LOQ* values for selected phenolic compounds calculated from the peak heights recorded by HPLC with UV and electrochemical detection. Conditions as in Figure 5, $E_D = +1.6$ V.

Parameter	detection	hydroquinone	phenol	*p*-cresol	*o*-cresol	4-CP	CMP
Retention time (min) (retention factor)	UV	1.28 (0.43)	2.48 (1.77)	3.36 (2.76)	3.73 (3.17)	4.32 (3.83)	6.28 (6.02)
	ED	1.42 (0.53)	2.63 (1.82)	3.52 (2.77)	3.88 (3.12)	4.47 (3.80)	6.44 (5.91)
LOD ($\mu mol L^{-1}$)	UV	0.16	0.21	0.23	0.33	0.29	0.31
	ED	0.21	0.07	0.21	0.16	0.18	0.22
LOQ ($\mu mol L^{-1}$)	UV	0.52	0.69	0.76	1.10	0.95	1.04
	ED	0.70	0.22	0.69	0.52	0.61	0.74

Abbreviations: 4-CP – 4-chlorophenol, CMP – 4-chloro-3-methylphenol.

than 1.5, which confirm successful differentiation of all eluted peaks (without any overlap) and prove that selected chromatographic conditions ensured high separation efficiency.

Optimization of the detection potential imposed on the working electrode was carried out within the potential range from +1.0 V to +1.8 V in steps of 0.1 V (Figure 5B). When detection potentials E_D higher than +1.6 V were applied on the working electrode, an increase in the background current along with baseline drifting and deformation of the first peak was observed. E_D of +1.6 V, which provided very low and stable background currents and the most convenient signal-to-background ratios for the analytes was chosen as optimal and used for all other HPLC-ED experiments. Additionally, the signal stability of all phenolic compounds was tested and within seven consecutive injections the *RSD* were 1.9–3.6 % and 2.0–3.8 % for peak areas and peak heights, respectively. Furthermore, the passivation of the O-BDD electrode surface was not observed due to the removal of possible fouling intermediates or reaction products by the stream of the mobile phase from the outlet of capillary.

Next, concentration dependences of the selected phenolic compounds were measured under optimized conditions. Parameters evaluated from both peak areas and peak heights recorded by UV and electrochemical detection systems are summarized in Table S1 of Supplementary material. The calculated *LOD* and *LOQ* values are shown in Table 3 and as it can be seen, electrochemical detection provided lower limits in case of five analyzed compounds, including *o*-cresol and *p*-cresol, in comparison with UV detection, hydroquinone being the only exception.

An achieved *LOD* value of 0.21 $\mu mol L^{-1}$ for *p*-cresol by HPLC-ED with an O-BDD electrode with a B/C of 8000 ppm in a "wall-jet" arrangement is similar or higher in comparison with *LOD*s obtained by employing other modified electrodes (see Table 1). Nevertheless, it should be pointed out that BDD electrodes possess sufficient sensitivity even without applying tedious modification procedures. In addition, the recorded responses on modified electrodes usually decrease with time, especially when an enzyme is included, thus the modification process has to be repeated, which can lead to the preparation of electrodes with altered performance, and therefore affecting the repeatability of measurements. On the other hand, BDD electrodes can be easily electrochemically activated *in-situ*, which ensure not only resistance to surface passivation but also stable responses and very good repeatability of the obtained signals. For *o*-cresol, a *LOD* value of 0.16 $\mu mol L^{-1}$ was obtained by HPLC-ED and this easily outperforms the only voltammetric method used for *o*-cresol determination found in the literature [61] (see Table 1).

3.4 Voltammetric and Amperometric Determination of *o*- and *p*-cresol and Other Phenolic Compounds in River Water

To verify the applicability of the developed procedure, determination of selected phenolic pollutants was performed in river water samples. No signals of studied analytes or other electroactive species were detected in the collected and subsequently filtered and diluted (see section 2. Material and Methods) river water samples, thus the samples were spiked by a known concentration (10.5 $\mu mol L^{-1}$) of phenolic compounds and analyzed by the standard addition method (Figure 6). Table 4 summarizes the measured concentrations by HPLC-ED and HPLC-UVD methods along with the confidence interval $L_{1,2}$ and *RSD*, and as evidenced analyzed phenolic compounds were determined with sufficient accuracy and precision.

Regarding HPLC-ED measurements, assessed recoveries based on peak heights were found to be satisfactory within the range from 92.9 % to 104.5 % for all spiked phenolic compounds. Recoveries calculated from the peak areas were in the range of 98.8 %–102.6 % for five phenolic analytes in the mixture (phenol, *p*-cresol, *o*-cresol, 4-chlorophenol, 4-chloro-3-methylphenol) and hydroquinone recovery was 78.9 %.

On the contrary, in HPLC-UVD chromatogram of the river water sample a signal of an unknown compound interfered with a hydroquinone peak resulting in lower recovery values of 67.7 % and 82.3 % evaluated from peak areas and peak heights, respectively. For other phenolic compounds presented in the spiked water sample, recov-

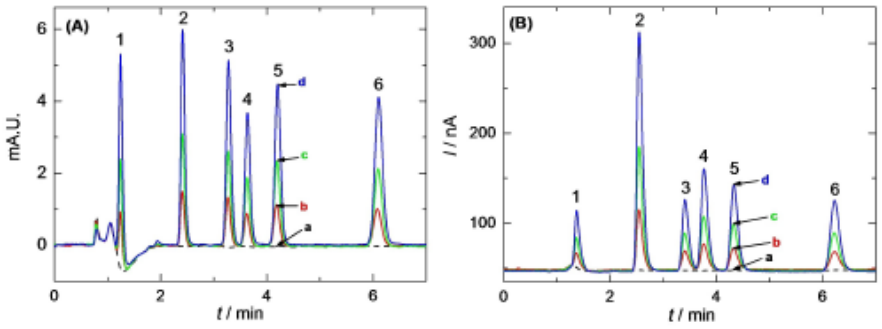

Fig. 6. Chromatograms of filtered and diluted river water samples: (a) blank, and spiked with the concentration of selected phenolic compounds of (b) 10.5 μmol L^{-1}, (c) 20 μmol L^{-1}, and (d) 40 μmol L^{-1} recorded using (A) UV detection at $\lambda = 280$ nm and (B) electrochemical detection with anodically activated BDD electrode of B/C 8000 ppm with applied detection potential $E_D = +1.6$ V. Analytes eluted as follows: (1) hydroquinone, (2) phenol, (3) *p*-cresol, (4) *o*-cresol, (5) 4-chlorophenol, and (6) 4-chloro-3-methylphenol. For chromatographic conditions see Figure 5.

Table 4. Determination of selected phenolic analytes in spiked river water samples using DPV and HPLC-ED using O-BDD electrode (B/C 8000 ppm, $E_D = +1.6$ V) and HPLC-UVD ($\lambda_D = 280$ nm). Calculated for a 95 % confidence level.

Analyte	Added c/μmol L^{-1}	Determined $c \pm L_{1,2}$/μmol L^{-1} (*RSD*)				
		HPLC-UVD		HPLC-ED		DPV
		Area	Height	Area	Height	Height
hydroquinone	10.50	7.11 ± 0.33 (3.72 %)	8.64 ± 0.44 (4.10 %)	8.28 ± 0.10 (0.93 %)	9.75 ± 0.20 (1.69 %)	
phenol	10.50	10.12 ± 0.16 (1.26 %)	10.52 ± 0.15 (1.18 %)	10.49 ± 0.24 (1.85 %)	10.54 ± 0.17 (1.28 %)	
p-cresol	10.50	10.58 ± 0.46 (3.52 %)	10.77 ± 0.15 (1.15 %)	10.77 ± 0.42 (3.17 %)	10.97 ± 0.25 (1.85 %)	10.45 ± 2.57 (9.91 %)
o-cresol	10.50	10.13 ± 0.18 (1.46 %)	10.32 ± 0.05 (0.38 %)	10.37 ± 0.28 (2.18 %)	10.44 ± 0.14 (1.11 %)	9.67 ± 1.80 (6.70 %)
4-chlorophenol	10.50	10.37 ± 0.26 (1.99 %)	10.65 ± 0.14 (1.03 %)	10.73 ± 0.20 (1.52 %)	10.74 ± 0.18 (1.37 %)	
4-chloro-3-methylphenol	10.50	10.30 ± 0.44 (3.47 %)	10.70 ± 0.33 (2.49 %)	10.55 ± 0.29 (2.21 %)	10.57 ± 0.21 (1.60 %)	

eries were found to be 96.4 %–100.8 % for peak areas and 98.3 %–102.6 % for peak heights. Clearly, when hydroquinone is expected to be in the analyzed river water samples, electrochemical detection is superior to UV detection as there is no interference from the environmental matrix.

Moreover, the accuracy of the proposed HPLC-ED method was evaluated by comparing with HPLC-UV method, as a reference technique. Paired Student *t*-test was applied to the acquired results for five analyzed phenolic compounds, hydroquinone was excluded from the test due to the matrix effects occurring in HPLC-UVD chromatograms. The calculated *t* values were smaller than the critical value (2.78, $\alpha = 0.05$), thus results obtained by HPLC coupled with both UV and electrochemical detectors are not statistically significant at a confidence interval of 95 % for phenol, *p*-cresol, *o*-cresol, 4-chlorophenol and 3-methyl-4-chlorophenol.

The optimized DPV method developed in this study (see Section 3.2) was also applied for determination of the studied cresol isomers in treated spiked river water samples and satisfactory values of recovery were obtained, 99.5 % and 92.1 % for *p*-cresol and *o*-cresol, respectively. This method exhibits lower precision in comparison with HPLC-ED, as is obvious from *RSD* values in Table 4. Another and substantial drawback is the fact that by using DPV, *o*- and *p*-cresol cannot be detected simultaneously due to overlapping oxidation peaks; the peak potential difference of 10 mV (see Figure 4) is insufficient.

4 Conclusion

This study presents differences in electrochemical behavior of *o*-cresol and *p*-cresol on carbon-based electrode materials and develops strategies for their detection using *tn-sttu* activated BDD electrode. Cresol isomers were

found to be oxidized by mechanisms as other phenolic compounds on O-terminated and polished BDD electrodes, and other common carbon-based electrode materials including CPE, PGE, and GCE. Formation of reaction products (hydroquinones/quinones) is coupled with creation of dimers and polymeric films on the electrode surface as a result of mutual reaction of reaction intermediates such as radicals and radical cations. Structure differences of these intermediates resulting from a variety of mesomeric forms of the cresol isomers leads to different structures of reaction products possessing higher proclivity to adsorption for *o*-cresol than *p*-cresol.

Further, O-terminated BDD electrodes with different boron doping levels (B/C content varying from 500 ppm to 8000 ppm) were used to optimize experimental conditions for detection of cresols using differential pulse and square-wave voltammetry. It was found that *o*-cresol and *p*-cresol exhibited comparable oxidation signal potentials in BR buffer (pH 2.0) and comparable *LOD*s for both compounds and methods tested in the range from 2.74 μmol L^{-1} to 0.79 μmol L^{-1}. Lower *LOD*s for *o*- and *p*-cresol and other phenolic pollutants in 10^{-7} mol L^{-1} concentration range were obtained for optimized HPLC-ED method applying oxidized BDD electrode (8000 ppm) as a working electrode in a wall-jet arrangement. The proposed voltammetric and HPLC-ED methods were successfully applied for determination of cresols in model river water samples and verified by an independent HPLC-UV method. The achieved *LOD* values are comparable with those in the literature, where a modification of electrode substrate or other type of electrode material was used. The application of different modifiers such as nanoparticles (metals, carbon nanotubes), biocomponents (enzymes) or polymeric films allows more sensitive and/or selective determination, but the preparation process of modified electrodes/biosensors is frequently tedious and complex.

The developed voltammetric and HPLC-ED procedures described in this paper provide a useful approach for fast, simple and sensitive determination of *o*- and *p*-cresol isomers involving an *in-situ* activation step to eliminate polymeric species from the electrode surface between individual measurements. This advantage of bare, non-toxic BDD electrodes justify their application in environmental analysis as a favored electrode material.

Acknowledgements

This research was carried out within the framework of Specific University Research (SVV 260560) and was supported by the Czech Science Foundation (project 20-03187S). JV thanks to the Grant Agency of Charles University (project GAUK 1390217). LS thanks to the Grant Agency of the Slovak Republic (grant No. 1/0159/20). Authors thank to Metrohm CZ (https://www.metrohm.com/cs-cz/) for valuable technical and intellectual support.

References

[1] WHO, *Guidelines for Drinking-water Quality: First addendum to Third Edition. Recommendations, 3th. ed.*, **2006**.
[2] M. Govindhan, T. Lafleur, B. R. Adhikari, A. C. Chen, *Electroanalysis* **2015**, *27*, 902–909.
[3] C. Flox, C. Arias, E. Brillas, A. Savall, K. Groenen-Serrano, *Chemosphere* **2009**, *74*, 1340–1347.
[4] M. S. Moneeb, I. I. Hewala, H. A. Elmongy, A. A. M. Wahbi, *Pak. J. Pharm. Sci.* **2015**, *28*, 1323–1330.
[5] C. Flox, E. Brillas, A. Savall, K. Groenen-Serrano, *Curr. Org. Chem.* **2012**, *16*, 1960–1966.
[6] V. Kavitha, K. Palanivelu, *Water Res.* **2005**, *39*, 3062–3072.
[7] C. W. Lee, J. Lee, J. Lee, H. Y. Eom, M. K. Kim, J. H. Suh, H. Yeom, U. Kim, J. R. Youm, S. B. Han, *J. Korean Chem. Soc.* **2009**, *30*, 2021–2026.
[8] S. A. Akgür, P. Özturk, Y. Kurtulmus, H. Karali, S. Ertürk, *Turk. J. Med. Sci.* **2001**, *31*, 415–419.
[9] S. Fustinoni, R. Mercadante, L. Campo, L. Scibetta, C. Valla, V. Foa, *J. Chromatogr. B* **2005**, *817*, 309–317.
[10] A. J. Cross, S. Boca, N. D. Freedman, N. E. Caporaso, W. Y. Huang, R. Sinha, J. N. Sampson, S. C. Moore, *Carcinogenesis* **2014**, *35*, 1516–1522.
[11] E. Sepetdjian, R. A. Halim, R. Salman, E. Jaroudi, A. Shihadeh, N. A. Saliba, *Nicotine Tob. Res.* **2013**, *15*, 1107–1112.
[12] T. Schettgen, A. Alt, P. Dewes, T. Kraus, *J. Chromatogr. B* **2015**, *995–996*, 93–100.
[13] A. Bahrami, A. Jonidi, B. Folladi, H. Mahjub, Q. Sadri, M. Motamedzade, *Pak. J. Biol. Sci.* **2005**, *8*, 1001–1005.
[14] S. Saha, R. Mistri, B. C. Ray, *Anal. Bioanal. Chem.* **2013**, *405*.
[15] J. Schlatter, A. Astier, *Biomed. Chromatogr.* **1995**, *9*, 302–304.
[16] G. Feroci, A. Fini, G. Fazio, P. Zuman, *J. Colloid Interface Sci.* **1996**, *178*, 339–347.
[17] J. P. Folley, *J. Chromatogr.* **1988**, *441*, 347–354.
[18] E. Nieminen, P. Heikkila, *J. Chromatogr.* **1986**, *360*, 271–278.
[19] L. Segovia-Martínez, Y. Molinder-Martinez, L. Campíns-Falcó, *J. Chromatogr. A*, **2010**, *1217*, 7926–7930.
[20] G. Achilli, G. P. Cellerino, G. M. Deril, S. Bird, *J. Chromatogr. A* **1995**, *697*, 357–362.
[21] A. Asan, I. Isildak, *J. Chromatogr. A* **2003**, *988*, 145–149.
[22] J. Czuczwa, C. Leuenberger, J. Tremp, W. Giger, M. Ahel, *J. Chromatogr.* **1987**, *403*, 233–241.
[23] F. B. Reig, P. C. Falco, J. V. Andres, *J. Chromatogr. A* **1996**, *726*, 57–66.
[24] R. G. Dolatto, I. Messerschmidt, B. F. Pereira, R. Martinazzo, G. Abate, *Talanta* **2016**, *148*, 292–300.
[25] D. Vrsaljko, V. Haramija, A. Hadzi-Skerlev, *Electr. Power Syst. Res.* **2012**, *93*, 24–31.
[26] J. C. Wu, W. S. Rickert, A. Masters, *J. Chromatogr. A* **2012**, *1264*, 40–47.
[27] G. Boatto, M. Nieddu, A. Carta, A. Pau, S. Lorenzoni, P. Manconi, D. Serra, *Forensic Sci. Int.* **2004**, *139*, 191–194.
[28] L. Shu, J. Zhu, Q. Wang, P. He, Y. Fang, *Luminescence* **2014**, *29*, 579–585.
[29] M. F. Pistonesi, M. S. Di Nezio, M. E. Centurion, A. G. Lista, W. D. Fragoso, M. J. C. Pontes, M. C. U. Araujo, B. S. F. Band, *Talanta* **2010**, *83*, 320–323.
[30] M. L. Carreto, L. Lunar, S. Rubio, D. Perez-Bendito, *Analyst* **1996**, *121*, 1647–1652.
[31] R. G. Dolatto, I. Messerschmidt, B. F. Pereira, C. A. P. Silveira, A. Gilberto, *J. Braz. Chem. Soc.* **2012**, *23*, 970–976.

[32] T. Mafatle, T. Nyokong, *Anal. Chim. Acta* **1997**, *354*, 307–314.
[33] K. R. Saravanan, S. Sathyamoorthi, D. Velayutham, V. Suryanaraynan, *Electrochim. Acta* **2012**, *69*, 71–78.
[34] D. Rajkumar, K. Palanivelu, *Ind. Eng. Chem. Res.* **2003**, *42*, 1833–1839.
[35] N. Grootboom, T. Nyokong, *Anal. Chim. Acta* **2001**, *432*, 49–57.
[36] Y. C. Tsai, C. C. Chiu, *Sens. Actuators B* **2007**, *125*, 10–16.
[37] J. Adamski, P. Nowak, J. Kochana, *Electrochim. Acta* **2010**, *55*, 2363–2367.
[38] V. Carralero, M. L. Mena, A. Gonzales-Cortés, P. Yáñez-Sedeño, J. M. Pingarrón, *Biosens. Bioelectron.* **2006**, *22*, 730–736.
[39] Y. L. Zhou, J. F. Zhi, *Electrochem. Commun.* **2006**, *8*, 1811–1816.
[40] X. P. Zhu, S. Y. Shi, J. J. Wei, F. X. Lv, H. Z. Zhao, J. T. Kong, Q. He, J. R. Ni, *Environ. Sci. Technol.* **2007**, *41*, 6541–6546.
[41] X. Zhu, J. Ni, H. Li, Y. Jiang, X. A. Xing, A. G. L. Borthwick, *Electrochim. Acta* **2010**, *55*, 5569–5575.
[42] J. L. Nava, F. Nunez, I. Gonzáles, *Electrochim. Acta* **2007**, *52*, 3229–3235.
[43] K. Muzyka, J. R. Sun, T. H. Fereja, Y. X. Lan, W. Zhang, G. B. Xu, *Anal. Methods* **2019**, *11*, 397–414.
[44] N. J. Yang, S. Y. Yu, J. V. Macpherson, Y. Einaga, H. Y. Zhao, G. H. Zhao, G. M. Swain, X. Jiang, *Chem. Soc. Rev.* **2019**, *48*, 157–204.
[45] Š. Švorc, K. Cinkova, J. Sochr, M. Vojs, P. Michniak, M. Marton, *J. Electroanal. Chem.* **2014**, *728*, 86–93.
[46] J. Sochr, Š. Švorc, M. Rievaj, D. Bustin, *Diamond Relat. Mater.* **2014**, *43*, 5–11.
[47] Š. Švorc, J. Sochr, P. Tomčík, M. Rievaj, D. Bustin, *Electrochim. Acta* **2012**, *68*, 227–234.
[48] J. M. Freitas, T. D. Oliveira, R. A. A. Munoz, E. M. Richter, *Front. Chem.* **2019**, *7*, article number 190, DOI 10.3389/fchem.2019.00190.
[49] J. Iniesta, P. A. Michaud, M. Panizza, G. Cerisola, A. Aldaz, C. Comninellis, *Electrochim. Acta* **2001**, *46*, 3573–3578.
[50] J. Zavazalova, K. Prochazkova, K. Schwarzova-Peckova, *Anal. Lett.* **2016**, *49*, 80–91.
[51] J. Musilova, J. Barek, K. Peckova, *Electroanalysis* **2011**, *23*, 1236–1244.
[52] V. A. Pedrosa, S. A. S. Machado, L. A. Avaca, *Anal. Lett.* **2006**, *39*, 1955–1965.
[53] M. Narmadha, M. Noel, V. Suryanarayanan, *J. Electroanal. Chem.* **2011**, *655*, 103–110.
[54] G. W. Muna, N. Tasheva, G. M. Swain, *Environ. Sci. Technol.* **2004**, *38*, 3674–3682.
[55] L. A. Hutton, J. G. Iacobini, E. Bitziou, R. B. Channon, M. E. Newton, J. V. Macpherson, *Anal. Chem.* **2013**, *85*, 7230–7240.
[56] K. Schwarzová-Pecková, J. Vosáhlová, J. Barek, I. Šloufová, E. Pavlova, V. Petrák, J. Zavázalová, *Electrochim. Acta* **2017**, *243*, 170–182.
[57] G. F. Pereira, L. S. Andrade, R. C. Rocha-Filho, N. Bocchi, S. R. Biaggio, *Electrochim. Acta* **2012**, *82*, 3–8.
[58] R. A. Medeiros, R. C. Rocha-Filho, O. Fatibello-Filho, *Food Chem.* **2010**, *123*, 886–891.
[59] Y. L. Zhou, J. F. Zhi, *Electrochem. Commun.* **2006**, *8*, 1811–1816.
[60] S. Zhang, *Russ. J. Electrochem.* **2011**, *47*, 1257–1261.
[61] L. Fotouhi, M. Ganjavi, D. Nematollahi, *Sensors* **2004**, *4*, 170–180.
[62] K. Cizek, J. Barek, J. Fischer, K. Peckova, J. Zima, *Electroanalysis* **2007**, *19*, 1295–1299.
[63] J. Zima, H. Dejmkova, J. Barek, *Electroanalysis* **2007**, *19*, 185–190.
[64] T. A. Enache, A. M. Oliveira-Brett, *J. Electroanal. Chem.* **2011**, *655*, 9–16.
[65] M. Panizza, G. Cerisola, *Electrochim. Acta* **2003**, *48*, 3491–3497.
[66] M. Ferreira, H. Varela, R. M. Torresi, G. Tremiliosi-Filho, *Electrochim. Acta* **2006**, *52*, 434–442.
[67] S. Baluchova, A. Danhel, H. Dejmkova, V. Ostatna, M. Fojta, K. Schwarzova-Peckova, *Anal. Chim. Acta* **2019**, *1077*, 30–66.
[68] V. Suryanarayanan, M. Noel, *J. Electroanal. Chem.* **2010**, *642*, 69–74.
[69] L. Svorc, M. Rievaj, D. Bustin, *Sens. Actuators B* **2013**, *181*, 294–300.
[70] Y. Yardim, E. Keskin, Z. Senturk, *Talanta* **2013**, *116*, 1010–1017.
[71] S. A. Sundaram, S. K. Annamalai, *Electrochim. Acta* **2012**, *62*, 207–217.
[72] N. Vishnu, A. S. Kumar, *Anal. Methods* **2015**, *7*, 1943–1950.
[73] N. B. Tahar, A. Savall, *Electrochim. Acta* **2009**, *54*, 4809–4816.
[74] M. A. Q. Alfaro, S. Ferro, C. A. Martínez-Huitle, Y. M. Vong, *J. Braz. Chem. Soc.* **2006**, *17*, 227–236.
[75] C. Terashima, T. N. Rao, B. V. Sarada, D. A. Tryk, A. Fujishima, *Anal. Chem.* **2002**, *74*, 895–902.
[76] T. Zhang, Q. Lang, L. Zeng, T. Li, M. Wei, A. Liu, *Electrochim. Acta* **2014**, *115*, 283–289.
[77] R. Williams, pKa data compiled by R. Williams, accessed online on March 30, 2020. http://www.chem.wisc.edu/areas/reich/pkatable/pKa_compilation-1-Williams.pdf.
[78] M. Brycht, P. Lochynski, J. Barek, S. Skrzypek, K. Kuczewski, K. Schwarzova-Peckova, *J. Electroanal. Chem.* **2016**, *771*, 1–9.
[79] P. Yu, J. W. Zhang, T. Zheng, T. Wang, *Colloids Surf. A* **2016**, *494*, 241–247.
[80] P. de Lima-Neto, A. N. Correia, R. R. Portela, M. D. Juliao, G. F. Linhares, J. E. S. de Lima, *Talanta* **2010**, *80*, 1730–1736.

Received: April 1, 2020
Accepted: June 16, 2020
Published online on ■■, ■■

7.2 Publikace 2

Journal of Electroanalytical Chemistry 821 (2018) 111–120

Contents lists available at ScienceDirect

Journal of Electroanalytical Chemistry

journal homepage: www.elsevier.com/locate/jelechem

Voltammetric and adsorption study of 4-nitrophenyl-triazole-labeled 2′-deoxycytidine and 7-deazaadenosine nucleosides at boron-doped diamond electrode

Jana Vosáhlová[a], Lucie Koláčná[b], Aleš Daňhel[b], Jan Fischer[a], Jana Balintová[c], Michal Hocek[c,d], Karolina Schwarzová-Pecková[a], Miroslav Fojta[b,e,*]

[a] Charles University, Faculty of Science, Department of Analytical Chemistry, UNESCO Laboratory of Environmental Electrochemistry, Albertov 6, CZ-12843 Prague 2, Czech Republic
[b] Institute of Biophysics, Czech Academy of Sciences, Kralovopolska 135, CZ-61265 Brno, Czech Republic
[c] Institute of Organic Chemistry and Biochemistry, Czech Academy of Sciences, Flemingovo namesti 2, CZ-16610 Prague 6, Czech Republic
[d] Charles University, Faculty of Science, Department of Organic Chemistry, Hlavova 8, CZ-12843 Prague 2, Czech Republic
[e] Central European Institute of Technology, Masaryk University, Kamenice 753/5, CZ-62500 Brno, Czech Republic

ARTICLE INFO

Keywords:
Adsorption
Boron-doped diamond
Nitro compounds
Nucleoside labeling
Voltammetry

ABSTRACT

Electrochemical properties of 4-nitrophenyl triazole labeled 2′-deoxycytidine (dC^{TRNO2}) and 7-deazaadenosine (dA^{TRNO2}) were studied using alumina-polished boron doped diamond (BDD) electrode in acetate buffer pH 5.0. Cyclic voltammetry revealed peak-shaped signals for reduction of the nitro group at the potentials of ca −0.6 V (*vs.* Ag|AgCl|3 mol L^{-1} KCl reference electrode) and for the hydroxylamine/nitroso pair exhibiting quasi-reversible electron transfer at potentials comparable with redox processes of other nitro aromatic compounds at BDD electrodes. All electrochemical processes are directed by adsorption. Moreover, *ex situ* adsorption of dA^{TRNO2} and transfer to supporting electrolyte enables its quantitation using square wave voltammetry in small (several microliter) sample volumes after optimization of parameters for the hydroxylamine/nitroso redox couple. Competitive adsorption/desorption at the BDD surface was further studied by cyclic voltammetry with dA^{TRNO2} in the presence of electrochemically inactive phenyl triazole 7-deazaadenosine conjugate (dA^{TR}), revealing mutual displacement of both compounds at BDD surface. Further, the redox processes of simpler aromatic nitro compounds (4-nitrophenyl acetylene and 2-nitronaphthalene) are strongly affected when the BDD surface is covered by dA^{TR}.

1. Introduction

Boron doped diamond (BDD) is a modern but already well-established electrode material thanks to its advantageous mechanical and electrochemical properties as extreme hardness, high thermal conductivity, corrosion resistance, low background currents, and wide potential window, especially in the anodic region [1]. The continuing research has revealed fundamental differences in conductivity and electrochemical properties of BDD surface in dependence on its pre-treatment. Currently, anodic pretreatment using highly positive potentials in the region of water decomposition and introducing carbon-oxygen functionalities at the BDD surface is considered as the most stable mode, characterized by minimal surface conductivity and surface-confined polarity due to the polar $C^{\delta+}-O^{\delta-}$ bonds [2–4]. Hydrogen termination achieved by cathodic pretreatment in the region of hydrogen evolution and imparting high surface conductivity has been preferred for substances with reducible moieties e.g., azo compounds [5,6]. These *in situ* activation modes have been supplemented by mechanical polishing using alumina slurries or silk cloth. Such *ex situ* approach changes substantially the properties of BDD surface, as it leads to lower concentration of C—O—C, C═O, and C—OH groups and even absence of COOH groups in comparison with anodized surfaces [4,7]. Naturally, the proclivity of organic compounds to adsorption is influenced by the surface pre-treatment, as it changes substantially its polarity thus imparts hydrophilic or hydrophobic character. Originally, the hydrogen-terminated surfaces were considered to be resistive towards fouling due to their paraffin-like structure [8]. Nevertheless, this view has been overcome as substantial electrode fouling has been reported for some of the problematic moieties of organic compounds (causing severe fouling of other bare electrode materials as well), such

* Corresponding author at: Institute of Biophysics, Czech Academy of Sciences, Kralovopolska 135, CZ-61265 Brno, Czech Republic.
E-mail addresses: kpeckova@natur.cuni.cz (K. Schwarzová-Pecková), fojta@ibp.cz (M. Fojta).

https://doi.org/10.1016/j.jelechem.2018.01.003
Received 30 November 2017; Received in revised form 29 December 2017; Accepted 2 January 2018
Available online 03 January 2018
1572-6657/

as aromatic amino [9] or phenolic moieties [10–12]. In the last seven years, these findings draw attention to BDD as electrode material capable of adsorption of large biomolecules and their constituents and of organic compounds (especially phenolic and other flat aromatic compounds) and with variability in the surface structure depending on its pretreatment. In the case of methyl viologen (MV), adsorption of neutral, low polar form MV^0 was demonstrated on H-terminated BDD, but not at O-terminated surface [13]. Phenolic compounds in non-ionized form adsorb at O-terminated [14] or alumina-polished [15] BDD surface. Transfer stripping voltammetric methods were employed for the determination of vanillin [14,16] and chlorogenic, caffeic, and gallic acid [15].

Biomolecules and their constituents, known to adsorb at sp^2 carbon surfaces, have been studied by means of BDD-based materials. The knowledge of their adsorptive properties and electrochemical behavior can provide base for their analysis and further development of biosensors and bioassays for investigation of specific interactions with other (bio)molecules [17]. BDD surfaces with different termination have been employed for investigation of DNA, RNA and their constituents since 2002 [18–29], albeit in lesser extent compared to extensive literature on nucleic acid electrochemistry at sp^2 carbons [30]. Purine and pyrimidine bases as such seem not to adsorb at BDD surfaces regardless of the surface pretreatment [21,22]; nevertheless, Cu (I) complexes of the purines were reported to adsorb at O-terminated BDD surfaces [27]. Nucleotides and nucleosides exhibit proclivity to adsorption themselves or their electrochemical reaction products [19,25,31]. Nevertheless, all mentioned studies using the BDD electrode aim at detection of oxidative signals of guanine, adenine, or thymine. Reductive signals of the nucleobases appear at highly negative potentials and they are typically connected to electroreduction of cytosine and adenine (usually giving a single "peak CA") on mercury-based electrodes [30]. Recently some of us succeeded in detection of cathodic signals of thymine, adenine, uracil, and 5-methylcytosine in oligonucleotides at pyrolytic graphite electrode [32]. Introduction of reducible labels enables to study DNA and its components at a variety of electrode materials, advantageously at less negative potentials as demonstrated on hanging mercury drop, solid amalgam or pyrolytic graphite electrodes for anthraquinone [33], 3-nitrophenyl [33–35], benzofurazan [34], aziclophenyl [36,37], 2,4-dinitrophenylhydrazine [38], and *N*-methyl-4-hydrazino-7-nitrobenzofurazane [39].

At BDD electrode, reduction of nitro group is the most frequently reported approach for electroanalysis of organic compounds in the region of negative potentials. Nitrophenols [40–45] and aminonitrophenols [46], nitro-group containing drugs (nitrofurazone [47], chloramphenicol [48], selected benzazepines [49]), and pesticides (methylparathion [50]), and derivatives of polycyclic aromatic hydrocarbons and heterocycles (1-nitropyrene [51], 3-nitrofluoranthene [52], 5-nitroquinoline [53]) were investigated at this electrode material.

This work aims at the investigation of electrochemical behavior of 4-nitrophenyl triazole labeled nucleosides 2′-deoxycytidine (dC^{TRNO2}) and 7-deazaadenosine (dA^{TRNO2}; structures in Fig. 1) at BDD electrode by means of voltammetric techniques. Electrochemical reduction of nitro group, as well as redox activity of the hydroxylamine/nitroso moieties represent a base for quantitation of these labeled nucleosides, as well as for studies on their adsorption at the BDD surface. As potential competitive adsorbents electrochemically inactive analog dA^{TR} not possessing the nitro moiety as well as smaller-molecule organic nitro aromatics were employed to compare their adsorbability at the BDD electrode with that of the nucleoside conjugates.

2. Experimental

2.1. Reagents and solutions

dC^{TRNO2}, dA^{TRNO2} and dA^{TR} nucleosides were prepared according to previously published protocols [54]. Their stock solutions in dimethyl sulfoxide (c = 1.36 mmol L^{-1}) were stored at − 20 °C. Stock solutions of 4-nitrophenyl acetylene and 2-nitronaphthalene were prepared in dimethyl sulfoxide at the concentration of 4.08 mmol L^{-1}. Supporting electrolyte, 0.2 mol L^{-1} acetate buffer pH 5.0, was prepared by mixing sodium acetate and acetic acid. Alumina (0.5 μm) polishing kit was supplied by Elektrochemické detektory, Turnov, Czech Republic. Nitrogen (Nitrogen 4.0, Linde Gas, Czech Republic) was used for removing oxygen from studied solutions. Acetic acid, sodium acetate, dimethyl sulfoxide (all p.a. purity) were purchased from local producers, Czech Republic.

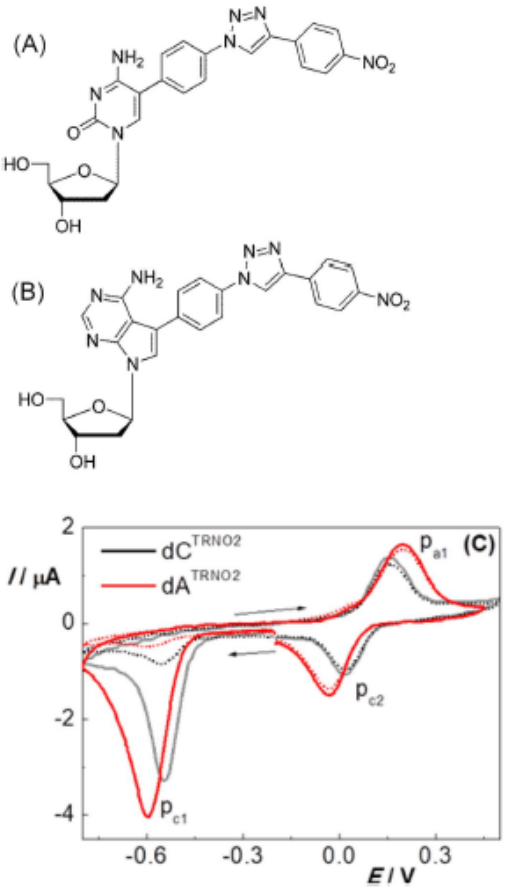

Fig. 1. Structural formulas of (A) dC^{TRNO2} and (B) dA^{TRNO2}, and (C) their cyclic voltammograms (dC^{TRNO2} – black line; dA^{TRNO2} – red line, the first (solid) and the second (dashed) scan. Concentration of analytes 1 × 10^{-5} mol L^{-1} of each, supporting electrolyte 0.2 mol L^{-1} acetate buffer pH 5.0, scan rate 0.5 V s^{-1}. Initial potential − 0.2 V, switching potentials − 0.8 V and + 0.4 V. Peak p_{c1} – reduction of $-NO_2$, peak p_{a1} – oxidation of –NHOH, peak p_{c2} – reduction of –NO. (For interpretation of the references to colour in this figure legend, the reader is referred to the web version of this article.)

2.2. Instrumentation

The cyclic voltammetry (CV) and square wave voltammetry (SWV) were carried out using Autolab PGSTAT101 (Metrohm, Switzerland)

driven by Nova 1.11 software. All measurements were performed in the three-electrode setup with Ag|AgCl (3 mol L^{-1} KCl) as a reference electrode and platinum wire as an auxiliary electrode (both from Elektrochemické detektory, Turnov, Czech Republic). Boron doped diamond working electrode with disk diameter of 3.0 mm (geometric area 7.1 mm^2, B/C ratio in gaseous phase during the deposition step 1000 ppm) was purchased from Windsor Scientific, UK.

2.3. Voltammetric procedures

The BDD surface was activated by alumina polishing (a slurry of the 0.5 μm alumina for 15 s) between individual measurements to prevent negative consequences of its passivation caused by strong sample adhesion. 0.2 mol L^{-1} acetate buffer pH 5.0 was used as supporting electrolyte, measurements were carried out at room temperature in the volume of 2 mL. Samples were diluted to the tested concentration by supporting electrolyte on the day of measurement. Peak-current values (I_p) were evaluated from the line connecting current minima at both sides of the voltammetric peak. All the solutions were degassed by 5 min passing nitrogen

Generally, two approaches were employed to study the electrochemical behavior of dA^{TRNO2} and dC^{TRNO2}. *In situ* voltammetry means direct recording of voltammograms in solution of each substance in supporting electrolyte. It was performed immediately after immersion of the polished electrode in the measured solution or after 15 s accumulation at open circuit of the studied substance. For transfer (*ex situ*) voltammetry, sample accumulation at the electrode surface was applied. BDD electrode was dipped in the sample solution in supporting electrolyte for 15 s (if not stated otherwise), washed twice in distilled water and consequently transferred to supporting electrolyte for measurement. Cyclic voltammograms were recorded at the scan rate of 0.5 V s^{-1} in the potential range from − 0.8 V to + 0.45 V with − 0.2 V as starting potential for cathodic scan and without any electrode activation between individual scans, if not stated otherwise. Frequency (f), amplitude (A) and step potential of the staircase waveform (ΔE) were optimized parameters in SWV for the –NHOH/–NO redox couple. The SWV anodic scan from − 0.8 V to + 0.45 V was performed after 15 s accumulation of dA^{TRNO2} at open circuit followed by 2 s reduction at − 0.8 V.

The concentration dependences were constructed from the average of four replicate measurements for each concentration of dA^{TRNO2} and were evaluated by the least squares linear regression method. For cyclic voltammetry, the limits of detection (LOD) were calculated as a threefold of the standard deviation s of the peak currents (ten runs) of the lowest measurable concentration, divided by the slope of corresponding calibration curve k. Competition experiments were performed by transferring one of the analytes (by dipping the BDD electrode for 15 s to the analyte solution in supporting electrolyte, followed by double wash in distilled water) to the supporting electrolyte containing the other analyte.

3. Results and discussion

3.1. In situ cyclic voltammetry of dA^{TRNO2} and dC^{TRNO2} nucleosides

Cyclic voltammetry of dA^{TRNO2} and dC^{TRNO2} nucleosides was firstly performed *in situ*; *i.e.*, in 1×10^{-5} mol L^{-1} solution of either of the substances in 0.2 mol L^{-1} acetate buffer pH 5.0 with vertex potentials of − 0.8 V and + 0.45 V (which are right next to the bases of the observed cathodic and anodic peaks). The negative vertex potential of − 0.8 V is close to the onset of supporting electrolyte caused by hydrogen evolution, but still well within the potential window of BDD electrode. Thus this choice of vertex potentials ensures stability of the polished surface and prevents it from anodic oxidation or cathodic hydrogenation. For both substances, typical signals for nitro group reduction were observed (Fig. 1). In the first cathodic scan, a single cathodic peak p_{c1} corresponding to the four-electron reduction of nitro group to hydroxylamino group (Eq. 1) appears at the potential of − 0.60 V (for dA^{TRNO2}) and − 0.55 V (dC^{TRNO2}):

$$ArNO_2 + 4e^- + 4H^+ \rightarrow ArNHOH + H_2O \quad (1)$$

In the reverse anodic/second cathodic scan a pair of anodic peak p_{a1} and cathodic peak p_{c2} centred about the potential ca + 0.10 V corresponds to the two electron – two proton quasireversible redox system of hydroxylamino group (ArNHOH) and nitroso group (ArNO) (Eq. 2):

$$ArNHOH \leftrightarrow ArNO + 2e^- + 2H^+ \quad (2)$$

This assumption is based on a number of studies devoted to the mechanism of reduction of aromatic nitro compounds at various electrode materials [55,56]. Thus, formation of corresponding nitroso and hydroxylamino derivatives of deoxyadenosine dA^{TRNO}, dA^{TRNHOH} and deoxycitidine dC^{TRNO}, dC^{TRNHOH} is expected. The reduction potentials of the nitro group of tested labeled nucleosides are comparable [49,53] or slightly less negative [46,51] than those obtained for other nitro aromatic compounds at BDD electrodes in buffers of comparable pH values. In comparison with mercury-based electrodes the reduction of nitro group proceeds at more negative potentials, also for other previously studied nucleosides and nucleotides labeled by a nitro group-containing moiety, *e.g.*, 3-nitrophenyl [33,35], 2,4-dinitrophenylhydrazine [38], or *N*-methyl-4-hydrazino-7-nitrobenzofurazan [39]. In the latter studies, the reported reduction potential of the nitro moiety − 0.45 V in ammonium formate – phosphate buffer pH 6.9, *i.e.*, media more basic than the acetate buffer pH 5.0 used in the current study suggests the peak potential difference of about 0.2 V–0.3 V between BDD and mercury-based electrodes. Thus, as for many other redox processes at the heterogeneous surface of BDD, the electron transfer at this material is hindered [57] which leads to more negative potentials for reduction of nitro group.

Interestingly, the peaks arising from redox reaction of the –NHOH/–NO couple are symmetric with peak potential difference ΔE_p between potential of the anodic peak and cathodic peak of 0.23 V for dA^{TRNO2} and 0.14 V for dC^{TRNO2}. In general, characteristics of these peaks nearing the parameters reversible redox systems are known for mercury surfaces (*e.g.*, m-AgSAE [55,58]) rather than for BDD surfaces, where the signals of this redox couple are characterized by broadened shape and large peak potentials separation, even of several hundreds of millivolts [48,53] (compare also cyclic voltammograms of 2-nitronaphtalene and 4-nitrophenyl acetylene in Fig. S3 in Supplemental materials). For the tested labeled nucleosides the peak-shaped CV signals and their stability during repetitive potential cycling indicates their adsorption at BDD surface. The peak potential and height differences for the peaks p_{c1} assigned to nitro group reduction and –NHOH/–NO (p_{a1}/p_{c2}) redox couple in dA^{TRNO2} and dC^{TRNO2} can be attributed different adsorbabilities of the two conjugates at BDD surface, favoring easier electron transfer for dC^{TRNO2} with less negative E_p for nitro group reduction (p_{c1}) and lower peak-to-peak separation for p_{a1}/p_{c2} redox couple. On the other hand, comparison of cytosine and 7-deazaadenine nucleoside triphosphates modified by anthraquinone moiety resulted in more facile electron transfer at HMDE for the latter base [33], indicating the importance of the structure of side chain attached to the nucleobase on the adsorption capability and structure of the adsorbed layer, influencing the electron transfer. The adsorption of dA^{TRNO2} at BDD surface was further confirmed by linear dependences of the peak heights I_p on the scan rate v (see Fig. S1 and Table S1 summarizing the parameters of the linear dependences in Supplemental materials) for all observed peaks. This scan rate and further studies were performed only with dA^{TRNO2}, since the described qualitative difference in voltammetric signals of both labeled nucleosides is insignificant and thus dA^{TRNO2} was considered as typical representative of nitro group labeled nucleosides with sufficient solution stability.

3.2. *Ex situ* voltammetry of dA^{TRNO2}

Strong adhesion of dA^{TRNO2} and products of its electrochemical transformation to the electrode surface was further utilized in *ex situ* voltammetric techniques, which comprise adsorption of the substance at the BDD surface from a suitable medium (here, the background electrolyte solution was used), its transfer and recording of the voltammogram in blank supporting electrolyte. This technique has been previously denoted as transfer stripping voltammetry, nevertheless, the term "stripping" is problematic in the case of dA^{TRNO2} due to its strong adsorption at the BDD surface and stability of the adsorbed layer with minimal desorption during potential cycling when the electrode is immersed in supporting electrolyte in absence of other strongly adsorbing species. The robust and mechanical stable BDD electrode represents an ideal tool for such approach taking the advantage of easy handling, and further low sample consumption and minimizing of possible matrix effects due to the transfer procedure involving washing step.

At first, the time of *ex situ* accumulation t_{acc} of dA^{TRNO2} ($c = 1 \times 10^{-5}$ mol L^{-1}) at BDD surface at open circuit from supporting electrolyte was optimized with the t_{acc} maximum of 30 s. An gradual increase of intensities of all redox signals p_{c1}, p_{a1}, and p_{c2} is obvious in Fig. 2 depicting the first two cycles of CVs of dA^{TRNO2} recorded after transfer of the BDD electrode to supporting electrolyte. Importantly, the signal of nitro group reduction p_{c1} is practically missing in the second scan indicating complete reduction of the adsorbed substance. A minimal current increase for longer accumulation than 15 s was observed for all three signals, thus t_{acc} was used in further studies.

A comparison of the first two cycles for *in situ* and *ex situ* cyclic voltammetry of dA^{TRNO2} is further depicted in Fig. 3 and evaluation of peak heights of all peaks p_{c1}, p_{a1}, and p_{c2} for ten consecutive cycles in Fig. 4. CVs were recorded at two concentrations of dA^{TRNO2}, representing complete coverage of the surface ($c = 1 \times 10^{-5}$ mol L^{-1}) and partially covered surface for concentration in the steepest part of the calibration dependence ($c = 2 \times 10^{-6}$ mol L^{-1}; for details see Section 3.3).

The most important features are as follows: (i) For nitro group reduction the peak potential is constant ($E_{pc1} \sim -0.58$ mV). For *in situ* mode (red dependences in Fig. 4A,B), a decline of ca 99% and ca 95% is observable between the first and the tenth cycles for the higher and lower concentration of dA^{TRNO2} with substantial decrease of ca 91% and 94%. between the first and the second CV scan. For *ex situ* mode

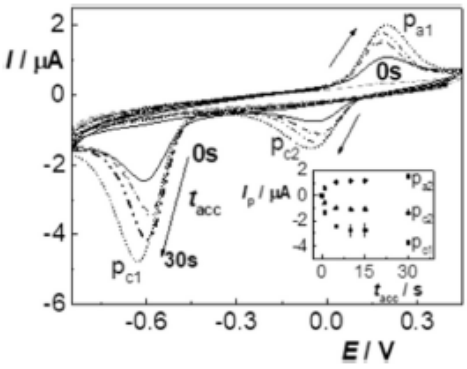

Fig. 2. *Ex situ* CV responses of dA^{TRNO2} measured in 0.2 mol L^{-1} acetate buffer pH 5.0, time of accumulation (t_{acc}) of dA^{TRNO2} ($c = 1 \times 10^{-5}$ mol L^{-1}) from supporting electrolyte solution: 0 s, 1 s, 5 s, 10 s, 15 s, 30 s. Inset: Peak heights I_p evaluated from the same experiments: (peak p_{c1},▼) reduction of $-NO_2$, (peak p_{a1}, ●) oxidation of –NHOH, (peak p_{c2}, ▲) reduction of –NO. Initial potential −0.4 V, switching potentials −0.8 V and + 0.45 V, scan rate 0.5 V s^{-1}, the first and the second scan depicted.

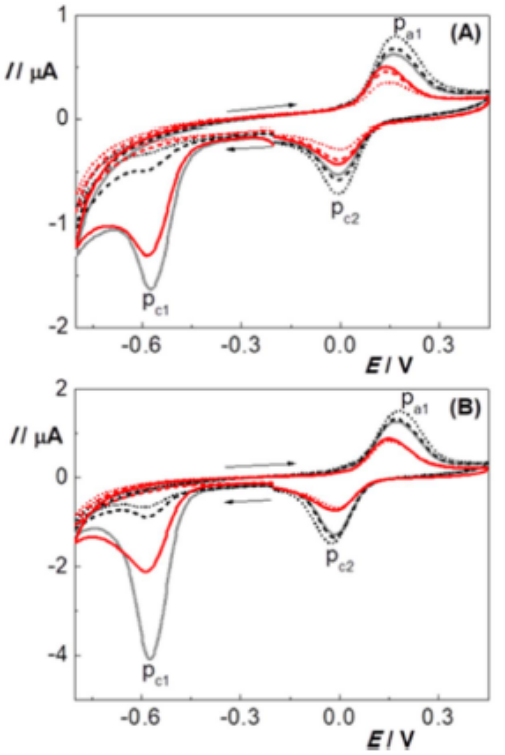

Fig. 3. *In situ* and *ex situ* cyclic voltammograms for different concentrations of dA^{TRNO2}. Black lines – *in situ* CVs of dA^{TRNO2} in supporting electrolyte containing the analyte. Red line – CVs of dA^{TRNO2} after *ex situ* accumulation (t_{acc} = 15 s) of dA^{TRNO2} from supporting electrolyte. Concentration of dA^{TRNO2}: (A) 2×10^{-6} mol L^{-1}, (B) 1×10^{-5} mol L^{-1}. The first (solid), the second (dashed), and the tenth (dotted) scan. Supporting electrolyte 0.2 mol L^{-1} acetate buffer pH 5.0, scan rate 0.5 V s^{-1}. Initial potential −0.2 V, switching potentials −0.8 V and + 0.45 V. Specification of signals (p_{c1}, p_{a1}, and p_{c2}) in Fig. 1. (For interpretation of the references to colour in this figure legend, the reader is referred to the web version of this article.)

(pink dependences in Fig. 4A, B), when no dA^{TRNO2} is present in the solution, the p_{c1} is practically missing in the second and consecutive scans indicating complete reduction of the adsorbed dA^{TRNO2} at the BDD surface.

(ii). The dA^{TRNHOH}/dA^{TRNO} redox couple has constant peak potential of ca + 0.1 V for the reduction of dA^{TRNO} (p_{c2}) for both modes and concentrations of dA^{TRNO2}, but a peak potential shift to less positive values is obvious for the dA^{TRNHOH} oxidation (p_{a1}) in *ex situ* mode, thus changing the peak-to peak separation from + 0.17 V (*in situ* CV) to + 0.14 V (*ex situ* CV) (Fig. 3). Thus, the oxidation of dA^{TRNHOH} stably adsorbed at BDD surface is facilitated in the absence of dA^{TRNO2} in solution and/or weakly interacting molecules which are removed by washing. Presumably, the mutual interactions of dA^{TRNHOH} already adsorbed at the surface and dA^{TRNO2} in the solution aspiring to be adsorbed in the *in situ* mode disables partially the electronic communication between the dA^{TRNHOH} molecules and the electrode surface and thus more positive potential for the *in situ* than *ex situ* mode is observed.

(iii). Remarkable stability of the peak heights for dA^{TRNHOH}/dA^{TRNO} (p_{a1}/p_{c2}) redox couple upon repetitive cycling is obvious for

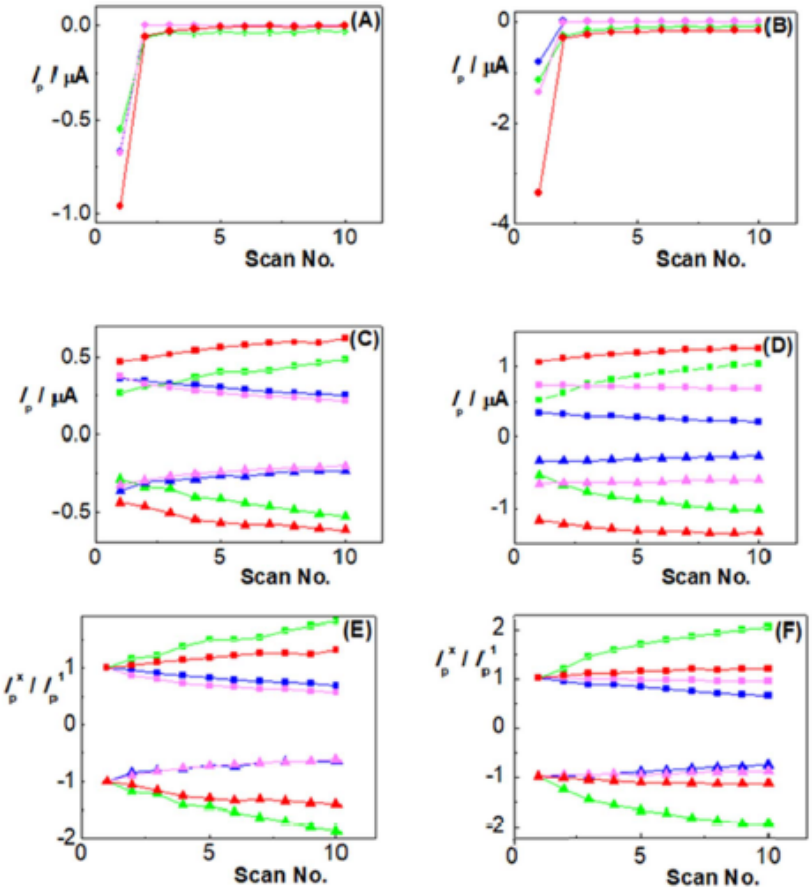

Fig. 4. Dependence of peak height I_p of dA^{TRNO2} on number of scans in cyclic voltammetry for peak p_{c1} (reduction of $-NO_2$ group (●), A + B) and for peaks p_{a1}/p_{c2} (redox couple –NHOH (■)/–NO (▲), C-F) of dA^{TRNO2} depicting real I_p values (C + D) or I_p^x/I_p^1 ratio (E + F), where x refers to the number of cycle. dA^{TRNO2} concentration (A + C + E) 2×10^{-6} mol L^{-1} or (B + D + F) 1×10^{-5} mol L^{-1}. Measurements were performed for different arrangements with dA^{TRNO2} analyte and dA^{TR} competitor (see part 3.4 for details): Red – dA^{TRNO2} in supporting electrolyte, bare BDD electrode; pink – CVs with dA^{TRNO2} *ex situ*-accumulated at BDD electrode, transfer to blank electrolyte; green – BDD electrode with *ex situ*-accumulated dA^{TR}, dA^{TRNO2} in supporting electrolyte; blue – BDD electrode with *ex situ*-accumulated dA^{TRNO2}, dA^{TR} in supporting electrolyte. *Ex situ* accumulation of dA^{TR} was always performed for 1×10^{-5} mol L^{-1} substance in supporting electrolyte, t_{acc} = 15 s. (For interpretation of the references to colour in this figure legend, the reader is referred to the web version of this article.)

1×10^{-5} mol L^{-1} concentration of dA^{TRNO2}, *i.e.* for covered surface in the *ex situ* mode (CVs in Fig. 3B and pink symbols in the Fig. 4D,F) and for the *in situ* mode (CVs in Fig. 3B and red symbols in the Fig. 4D,F). Only a slight decline/increase of peak heights can be traced for *ex situ*/*in situ* mode on I_p *vs.* scan number dependences depicted with absolute (Fig. 4D) and relative (Fig. 4F) peak current values. On one hand, very strong adsorption of dA^{TRNHOH} and dA^{TRNO} conjugates results in minimal desorption, *i.e.* minimal decline (ca 9%) of p_{a1} and p_{c2} currents in blank supporting electrolyte solution (*ex situ* mode), on the other hand in minimal p_{a1} and p_{c2} currents increase (ca 14%) in dA^{TRNO2} containing supporting electrolyte (*in situ* mode). In this case, the potentially desorbed molecules can be replaced by dA^{TRNO2} present in the solution or products of subsequent redox reactions thus keeping the possibility for minimal current increase in subsequent cycles, and also for appearance of the "residual" irreversible peak p_{c1} on repeated CV scans. Nevertheless, it should be emphasized that the observed current changes are minimal indicating very strong adsorption of the dA^{TRNHOH}/dA^{TRNO} molecules.

For partially covered BDD surface (*i.e.*, 2×10^{-6} mol L^{-1} concentration of dA^{TRNO2}; CVs in Fig. 3A and red symbols (*in situ* mode) and pink symbols (*ex situ* mode) in the Fig. 4C,E) the situation is somewhat different. The above mentioned trends are more pronounced and the peak currents for dA^{TRNO} and dA^{TRNOH} in the tenth cycle are by ca 50%/35% lower/higher for the *ex situ*/*in situ* CV mode (Fig. 4E, relative scale of I_p). For the former case the gradual desorption from the partially covered BDD surface underlines the importance of intermolecular interaction of dA^{TR} derivatives to form stable layer at BDD surface. In the *in situ* mode the surface offers free area for redox reactions of dA^{TRNO2} from the bulk solution, and thus the signal of its reaction products dA^{TRNHOH} and dA^{TRNO} is gradually increasing, as these

products of primary reduction of dA^{TRNO2} remain in the adsorbed state.

3.3. Optimization of voltammetric techniques and concentration dependences

Cyclic voltammetry and square wave voltammetry were used for quantitation of the dA^{TRNO2} conjugate. Principally, the *ex situ* techniques with adsorption of the analyte at open circuit are more convenient in comparison with *in situ* techniques, as *ex situ* adsorption may prevent undesirable matrix effects and decreases sample consumption by both, substantially lower sample volume in microliter range needed for analysis and eventually, its reuse for repetitive adsorption of the analyte. Further, evaluation of capability of adsorption of tested species and their interaction with variety of other compounds in media used for recording of the voltammetric scan is a valuable approach, typically in analysis of DNA and its components [30]. For quantitation of dA^{TRNO2} the signal corresponding to nitro group reduction p_{c1} or to redox reactions of dA^{TRNHOH}/dA^{TRNO} (p_{a1}/p_{c2}) is applicable.

At first, the CV responses recorded at the scan rate of 500 mV s^{-1} at the potential of − 0.6 V in *in situ* and *ex situ* mode were evaluated to assess the p_{c1} signal of nitro group reduction. In both cases, 15 s accumulation of analyte at open circuit was applied. CV responses showed similar peak heights I_{pc1} and linear calibration dependences from 1.0 μmol L^{-1} to 100 μmol L^{-1} for both modes characterized by the following equations:

$$\textit{Instiu}\ \text{CV: } I_{pc1}\,(\mu\text{mol L}^{-1}) = 0.291 \pm 0.016\ c\ (\mu\text{mol L}^{-1}) - 0.153 \pm 0.093\ (R = 0.9935) \quad (3)$$

$$\textit{Exstiu}\ \text{CV: } I_{pc1}\,(\mu\text{mol L}^{-1}) = 0.155 \pm 0.014\ c\ (\mu\text{mol L}^{-1}) - 0.027 \pm 0.081\ (R = 0.9828) \quad (4)$$

The limits of detection (LOD) calculated as a threefold of the standard deviations of the peak currents (ten runs) of the lowest measurable concentration, divided by the slope of corresponding calibration curve are 0.15 μmol L^{-1} for the *in situ* and 0.03 μmol L^{-1} for the *ex situ* mode. Nevertheless, these detection limits are at least ten times lower than the lowest measurable concentration of 1.0 μmol L^{-1} for both modes, because of acceptable repeatability of peak heights for this concentration characterized by RSD of 15.0% (*in situ* mode) and 13.0% (*ex situ* mode). Thus, this concentration should be considered as the detection limit for practical purposes.

Our attention was further turned to the dA^{TRNHOH}/dA^{TRNO} redox couple, taking advantage of the quasireversible character of its CV response, for development of SWV methodology. Frequency, amplitude, and step potential of the staircase wave form were optimized for *in situ* anodic SWV scan in dA^{TRNO2} solution in 0.2 mol L^{-1} acetate buffer pH 5.0. Exactly, 15 s accumulation of dA^{TRNO2} at open circuit was followed by 2 s reduction at − 0.8 V (and thus generating dA^{TRNHOH}) and SWV anodic scan from − 0.8 V to + 0.45 V. During adjustment of the above mentioned parameters, each parameter was changed, while the others were kept constant. Frequency was investigated in the range of 5–200 Hz, amplitude from 10 mV to 150 mV and step potential in the range of 1–10 mV. As the latter parameter has minimal influence of the shape of SW voltammograms, it was kept at the value $\Delta E = 5$ mV during all optimizing experiments. The SWV responses for dA^{TRNHOH}/dA^{TRNO} redox couple and evaluation of the peak heights as a function of variation in f for constant value $A = 50$ mV are depicted in Fig. 5. The increase of f values promotes an increase of peak currents as results of increase of the scan rate, which is product of frequency and potential step in SWV measurements. Following the influence of the increase of f values on SW voltammograms in Fig. 5A, appearance of an indistinct second signal at + 0.03 V for $f \geq 60$ Hz on the shoulder of the main signal at the potential of + 0.10 V and increase of background current is obvious. Further, a parasitic third peak at ca − 0.1 V appears at the SW voltammograms. Despite the fact that only the lowest frequencies exhibited single symmetric signal, a higher frequency of 100 Hz was chosen for further optimization of A to ensure relatively short scanning period and prevent additional adsorption of the dA^{TRNO2} conjugate and its reduction product at BDD surface during the measurement in the case of the *in situ* mode. Fig. 6 depicts recorded SW voltammograms for amplitude A varied from 10 mV to 150 mV at $f = 100$ Hz and the net, forward, and backward components of the scan for $A = 10$ mV, 70 mV, and 150 mV are depicted in Supplemental materials in Fig. S2. Obviously, the backward current component is higher than the forward current component, which appears at more positive potential for $A \leq 110$ mV. This indicates that the coefficient transfer value α is lower than 0.5 for dA^{TRNHOH} oxidation as suggested by the SWV theory [59]. For further measurements the maximal value $A = 150$ mV resulting in the symmetric and highest signal was used together with frequency of 100 Hz and step potential of 5 mV.

Concentration dependence of the SWV peak height was measured in the dA^{TRNO2} concentration range of 0.25–10 μmol L^{-1}. It has a sigmoidal shape which confirms strong adsorption of the substance at the surface. Generally, the S-shaped course of the concentration dependences indicate intermolecular interaction at the surface, where certain coverage by the substance induces adsorption of more molecule and simultaneously, the rearrangement of the molecules at the surface can facilitate the oxidation/reduction process. At high concentration the saturation of concentration dependence indicates full coverage of the BDD surface. Such S-shaped dependences were typically reported for substances possessing the anthraquinone moiety, *e.g.*, 2-aminoanthraquinone, including base-modified cytosine and 7-deazaadenine nucleoside triphosphates [33] at HMDE.

3.4. Competitive adsorption/desorption experiments

The above data brought evidence of a strong adsorption of dA^{TRNO2} and products of its electrochemical transformations at the BDD electrode (manifested in a clear time-dependent accumulation at the electrode surface, resistance of its *ex situ* adsorbed layer towards medium exchange, and a remarkable stability of the signal of p_{a1}/p_{c2} pair in *ex situ* CV scans exhibiting quasi-reversible behaviour). In the following experiments we focused on competitive adsorption/desorption of dA^{TRNO2} at the BDD electrode surface in the presence of another adsorbing compound. As the competitor we chose phenyl triazole deoxyadenosine conjugate (dA^{TR}), a substance that differs from dA^{TRNO2} (see Fig. 1) only by absence of the active nitro group, thus being supposed to exhibit similar adsorption properties as dA^{TRNO2}. Expectably, CVs of dA^{TR} showed no CV signals in the potential range between − 0.8 V and + 0.45 V in both *in situ* (Fig. 8, green curves) and *ex situ* modes. When dA^{TR} was *ex situ*-adsorbed at the BDD surface (always from its 1×10^{-5} mol L^{-1} solution during 15-s accumulation time) and then CVs were recorded with such modified electrode in solution of dA^{TRNO2} (black curves in Fig. 8), signals of the latter compound were detected but the corresponding peak heights measured in the first CV scan were remarkably lower, compared to analogous measurements with bare BDD electrode (*e.g.*, peak p_{c1} current measured for $c = 1 \times 10^{-5}$ mol L^{-1} dA^{TRNO2} was depressed by a factor of 2.9. Repeated CV scanning resulted in a sharp drop in the peak p_{c1} current between 1st and 2nd scans in agreement with irreversibility of nitro group reduction (see above). On the other hand, heights of the quasi-reversible p_{a1}–p_{c2} pair gradually increased with the number of potential cycles (see 1st, 2nd and 10th cycles in Fig. 9 and dependences of I_p in Fig. 4 C + D). This peak current increase was relatively (compared to the values measured in 1st cycle) more significant than increase of the I_p values due to accumulation of dA^{TRNO2} (its reduction product) at the bare BDD electrode during repeated *in situ* CV (compare red and green symbols in Fig. 4). Such effects were observed for both 2×10^{-6} and 1×10^{-5} mol L^{-1} dA^{TRNO2}, for the higher analyte concentration being more pronounced (which in best visible from the plot of relative I_p^*/I_p^1 values, where I_{p1} is the respective peak height measured in 1st cycle

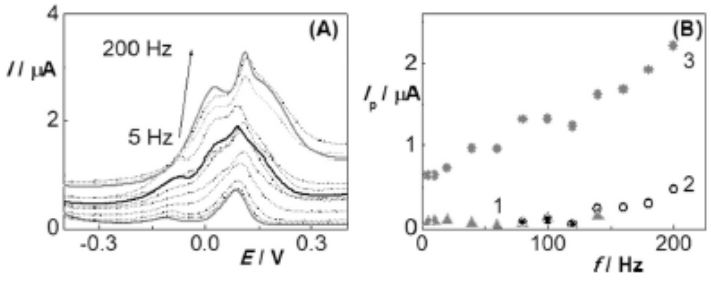

Fig. 5. Optimization of frequency f for *in situ* SWV for the –NO/–NHOH redox couple (peak p_{a1}/p_{c2}) of dA^{TRNO2} at bare BDD electrode. (A) SW voltammograms of dA^{TRNO2} for frequency 5 (bold line), 10, 20, 40, 60, 80, 100 (bold line), 120, 140, 160, 180, 200 (bold line) Hz and (B) dependence of peaks height I_p (at E_p (1) − 0.08 mV, (2) + 0.02 mV, and (3) + 0.10 mV) on frequency f. Supporting electrolyte 0.2 mol L^{-1} acetate buffer pH 5.0, amplitude A = 50 mV, potential step ΔE = 5 mV. The SWV anodic scan from − 0.8 V to + 0.45 V was performed after 15 s accumulation of dA^{TRNO2} at open circuit followed by 2 s reduction at − 0.8 V.

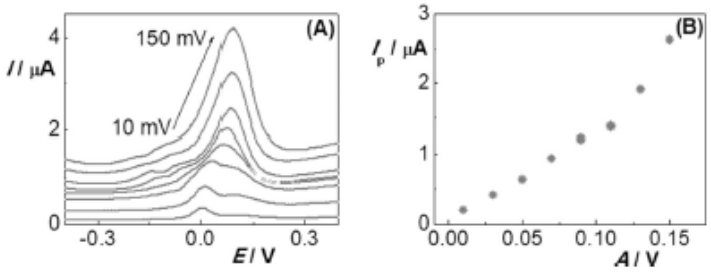

Fig. 6. Optimization of amplitude A for *in situ* SWV for the –NO/–NHOH redox couple (peak p_{a1}/p_{c2}) of dA^{TRNO2} at bare BDD electrode. (A) SW voltammograms of dA^{TRNO2} for amplitude 10, 30, 50, 70, 90, 110, 130, and 150 mV, and (B) dependence of peak height I_p on amplitude A. Supporting electrolyte 0.2 mol L^{-1} acetate buffer pH 5.0, frequency f = 100 Hz, potential step ΔE = 5 mV. Other conditions as in Fig. 5.

and x stands for the scan number, Fig. 4 E + F). Such behaviour suggests gradual exchange of the inactive dA^{TR} for active dA^{TRNO2} at the electrode surface and this process to be slow, in agreement with a strong adsorption of both species at the surface.

Analogous experiments were performed in an inverse arrangement *i.e.*, with dA^{TRNO2} *ex situ* pre-accumulated at the BDD electrode and the dA^{TR} in background electrolyte solution during the CV scans (red curves in Fig. 8). First scans revealed lower peak currents when compared to values obtained in *ex situ* CV of dA^{TRNO2} measured in blank electrolyte (*e.g.*, by a factor of 1.7 for peak p_{c1} and 1×10^{-5} mol L^{-1} dA^{TRNO2} in solution) and during repeated CV scans the peak height were decreasing due to desorption of dA^{TRNO2} reduction products and/or their exchange for dA^{TR}. However, significant differences between trends in the peak p_{a1}/p_{c2} I_p values *versus* number of CV scans (up to 10) obtained for measurements in the absence and presence of dA^{TR} in the solution (compare pink and blue symbols in Fig. 4) were observed only for 1×10^{-5} mol L^{-1} dA^{TRNO2}, suggesting that in the case of 2×10^{-6} mol L^{-1} dA^{TRNO2} the major contribution to the observed I_p decrease came from desorption of dA^{TRNO2} reduction products without significant role of dA^{TR} in solution (which preferentially occupied free sites the surface incompletely covered with dA^{TRNO2}). On the other hand, exchange of dA^{TRNO2} reduction products for dA^{TR} got importance when concentration of the former compound was increased to 1×10^{-5} mol L^{-1}, resulting in nearly full coverage of the electrode with the pre-accumulated dA^{TRNO2} (see Fig. 4). Moreover, under the latter conditions we observed remarkable shifts of potentials of all three peaks in the directions of potential scans (Fig. 8 red curves), indicating that in the presence of dA^{TR} the corresponding redox processes became more difficult. Interestingly, no such effect was detected in the opposite arrangement, *i.e.*, with dA^{TR} pre-adsorbed at the BDD electrode and dA^{TRNO2} coming from the solution. Thus it seems that during exchange of dA^{TRNO2} for dA^{TR} some rearrangement of the dA^{TRNO2} adsorbed layer takes place, making the redox centre less accessible for communicating with active sites at the BDD surface and slowing down the electron transfer kinetics (more experimental work will be needed to clarify these phenomena).

As it can be concluded from the above experiments, both dA^{TRNO2} (and products of its primary reduction) and dA^{TR} exhibit comparable adsorbability at the BDD electrode which is, particularly at this type of electrode, unusually strong. Such strong adsorption can be related to rather complex structure of the nucleoside conjugates composed of deoxyribose, nucleobase and three extra aromatic rings (see Fig. 1). The high net adsorbability of the modified nucleosides can thus be ascribed to cumulative (and/or cooperative, see the S-shaped concentration dependence, Fig. 7) contributions of these moieties. In next experiments we used simple aromatic nitro compounds such as 2-nitronaphthalene and 4-nitrophenyl acetylene (the latter representing a building block of dA^{TRNO2} and dC^{TRNO2}). Importantly, none of these compounds gave measurable signals of the nitro group or products of its reduction in the *ex situ* mode of CV, suggesting their only weak interaction of the

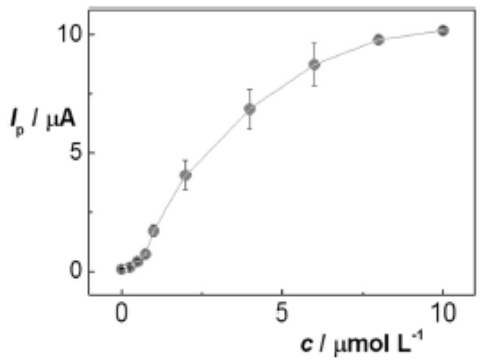

Fig. 7. Concentration dependence of –NHOH/–NO (p_{a1}/p_{c2}) redox couple of reduced dA^{TRNO2} evaluated from *ex situ* SW voltammograms: dA^{TRNO2} *ex situ* accumulated for 15 s at the BDD electrode at open circuit from supporting electrolyte, followed by transfer to supporting electrolyte, 2 s reduction and anodic SW scan from − 0.8 V to + 0.45 V. SWV parameters: frequency 100 Hz, amplitude 150 mV, potential step 5 mV. Supporting electrolyte 0.2 mol L^{-1} acetate buffer pH 5.0. The error bars are constructed as standard deviations (n = 4).

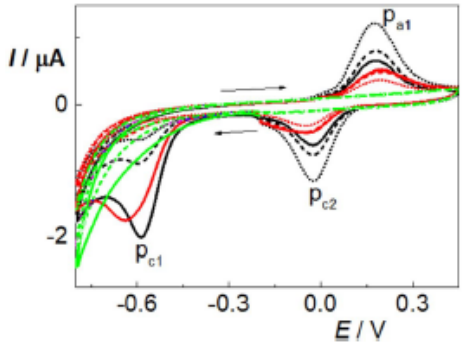

Fig. 8. Cyclic voltammograms for competition experiments of dA^{TRNO2} and dA^{TR} at BDD surface. Black lines – CVs with dA^{TR} *ex situ*-accumulated at the BDD electrode, measured in supporting electrolyte containing dA^{TRNO2} ($c = 1 \times 10^{-5}$ mol L^{-1}). Accumulation of dA^{TR} ($c = 1 \times 10^{-5}$ mol L^{-1}) for 15 s from supporting electrolyte solution. Red lines – CVs with dA^{TRNO2} *ex situ*-accumulated at the BDD electrode ($c = 1 \times 10^{-5}$ mol L^{-1}, $t_{acc} = 15$ s) measured in supporting electrolyte containing dA^{TR} ($c = 1 \times 10^{-5}$ mol L^{-1}). Green lines – CVs of dA^{TR} ($c = 1 \times 10^{-5}$ mol L^{-1}) in supporting electrolyte at bare BDD electrode. The first (solid), the second (dashed), and the tenth (dotted) scans are depicted. Supporting electrolyte 0.2 mol L^{-1} acetate buffer pH 5.0, scan rate 0.5 Vs^{-1}. Initial potential −0.2 V, switching potentials −0.8 V and +0.45 V. Specification of signals (p_{c1}, p_{a1}, p_{c2}) in Fig. 1. (For interpretation of the references to colour in this figure legend, the reader is referred to the web version of this article.)

electrode which did not resist the medium exchange. When measured *in situ* (solid curves in Fig. 9) both of them yielded well-developed peak p_{c1} due to nitro group reduction. On the other hand, the p_{a1}/p_{c2} pair was less well developed and showed remarkably higher ΔE_p 0.27 V or 0.47 V for 2-nitronaphthalene or 4-nitrophenyl acetylene, compared to 0.23 V obtained for dA^{TRNO2}). Moreover, during 10 repeated CV scans (Fig. S3 in Supplementary material) the peak p_{c1} height decreased with increasing number of scans less steeply than observed dA^{TRNO2} and tended to stabilization at about 53% (2-nitronaphthalene) and 42% (4-nitrophenyl acetylene) of values measured for the 1st scan. Heights of peaks p_{a1} and p_{c2} were increasing less significantly than observed for dA^{TRNO2}, particularly in the case of 4-nitrophenyl acetylene for which practically no change in I_p during the CV scanning was detected (Fig. S3). Taken together, these observations indicate a lack of (strong) adsorption of these two compounds and their reduction products at the BDD electrode.

Finally, we studied CV responses of 2-nitronaphthalene or 4-nitrophenyl acetylene at BDD electrode covered with *ex situ* pre-accumulated dA^{TR} (from its 1×10^{-5} mol L^{-1} solution for $t_{acc} = 2$, 15 or 30 s). Already after 2-s pre-accumulation of dA^{TR}, signals of both analytes exhibited E_p shifts in the direction of potential scans (dashed curves in Fig. 9). While peak p_{c1} remained relatively well measurable even when recorded at the dA^{TR}-modified BDD electrode, the p_{a1}/p_{c2} pair practically disappeared in the case of the 4-nitrophenyl acetylene and was (besides further increase in the ΔE_p value) strongly suppressed in the case of 2-nitronaphthalene. Prolonged accumulation of dA^{TR} caused further depression of the still measurable signals (Fig. 9), but the magnitude of changes observed between 2 and 30 s was much smaller than the difference between signals measured at bare BDD electrode and those obtained after 2-s dA^{TR} accumulation. Thus, the electrode coverage by dA^{TR} was almost complete after the shortest accumulation time. The observed effects suggest that while the reduction of nitro group can take place at the electrode surface covered by the strongly adsorbing inactive dA^{TR} (albeit with apparently slower electron transfer kinetics), redox processes of –NHOH/–NO corresponding to peaks p_{a1}/p_{c2} are under the same conditions strongly suppressed. Interestingly, 2-

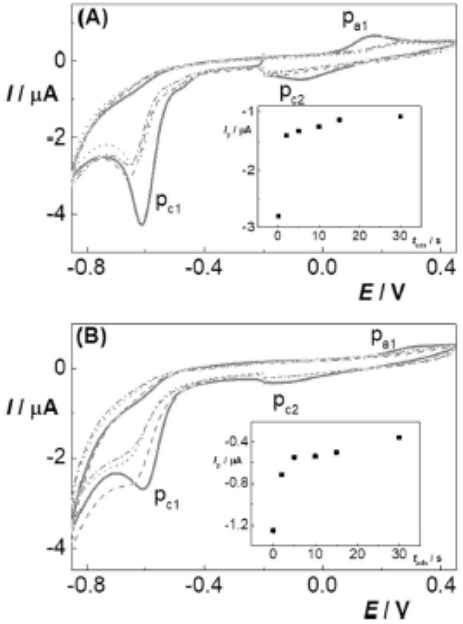

Fig. 9. Cyclic voltammograms for competition of dA^{TR} and (A) 2-nitronaphthalene and (B) 4-nitrophenyl acetylene at BDD surface. Solid lines: *In situ* cyclic voltammograms of (A) 2-nitronaphalene and (B) 4-nitrophenyl acetylene ($c = 1 \times 10^{-5}$ mol L^{-1} of each) measured at bare BDD electrode in supporting electrolyte. CVs with dA^{TR} *ex situ*-accumulated at the BDD electrode measured in supporting electrolyte containing (A) 2-nitronaphalene or (B) 4-nitrophenyl acetylene ($c = 1 \times 10^{-5}$ mol L^{-1} of each). dA^{TR} was adsorbed at BDD surface for 2 s (dash), 15 s (dot), 30 s (dash-dot) from its solution of c (dA^{TR}) $= 1 \times 10^{-5}$ mol L^{-1}. Scan rate 0.5 Vs^{-1} in 0.2 mol L^{-1} acetate buffer pH 5.0. In inset – corresponding dependences of peak p_{c1} height I_p on the time of accumulation t_{acc}.

nitronaphthalene possessing two condensed aromatic rings appears to be slightly more potent to break onto the electrode surface than 4-nitrophenyl acetylene with only one aromatic ring.

4. Conclusion

2′-Deoxycytidine and 7-deazaadenosine modified by 4-nitrophenyl triazole were studied by voltammetric techniques at boron doped diamond electrode in acetate buffer pH 5.0. Strong adsorption of these conjugates was revealed at the alumina-polished BDD surface, proved by peak-shaped signals of nitro group reduction and nitroso/hydroxylamino quasireversible redox couple with remarkable stability under repetitive cycling, linear dependences of their peak currents on the scan rate and even possibility of transfer of the labeled nucleoside *ex situ* adsorbed at the BDD surface. The potentials of the well-developed CV response of nitro group correspond or are slightly less negative than those of other nitro aromatic compounds at BDD electrodes [46,49,51,53], the highly stable response of the –NHOH/–NO redox couple with low peak potential difference of ca 0.2 V has not been virtually reported yet and can be used for quantitation of dA^{TRNO2} using anodic adsorptive transfer square wave voltammetry after *ex situ* accumulation of dA^{TRNO2} at BDD surface. This approach is rather unique, as up to now employment of transfer techniques with BDD electrode was reported only for phenolic compounds, mostly carboxylic acids in non-ionized form [14–16].

Further, we focused on adsorption/desorption studies to address the

importance of the structure of nucleoside conjugates composed of deoxyribose, nucleobase and three extra aromatic rings with attached nitro group. Unusually strong and fast adsorption was proved for all three 7-deazaadenine conjugates exhibiting redox activity (dA^{TRNO2}, dA^{TRNO}, dA^{TRNHOH}) at polished BDD electrode, as well as the nitro group lacking, thus electrochemically inactive conjugate dA^{TR}. Simpler aromatic nitro compounds (4-nitrophenyl acetylene and 2-nitronaphthalene) do not strongly adsorb at the BDD surface and the electron transfer for all investigated processes is depressed when the BDD surface is covered by dA^{TR}.

The strong adhesion of the tested strongly adsorbing nucleoside conjugates to the BDD surface suggest possibilities of their selective determination in mixtures with non-adsorbing or weakly adsorbing species, taking advantages of simple separation (and enrichment) at the electrode surface (in fact using a principle of adsorption chromatography). Naturally, applications in determination of 4-nitrophenyl triazole nucleos(t)ide conjugates (or other electroactive strongly adsorbing derivatives) in reaction mixtures during enzymatic processing of nucleic acids (*e.g.*, their consumption during incorporation by DNA polymerases or production during modified DNA cleavage with nucleolytic enzymes) can be envisaged and will be elaborated in following studies.

Acknowledgements

This research is carried out within the framework of Czech Science Foundation (project P206/12/G151). J.V. thanks to Specific University Research (SVV260440). Support from the the Academy of Sciences of the Czech Republic is acknowledged (RVO: 61388963 to L.K., M.F. and A.D., Praemium Academiae award for M. H.).

Appendix A. Supplementary data

Supplementary data to this article can be found online at https://doi.org/10.1016/j.jelechem.2018.01.003.

References

[1] K. Peckova, J. Musilova, J. Barek, Boron-doped diamond film electrodes - new tool for voltammetric determination of organic substances, Crit. Rev. Anal. Chem. 39 (2009) 148–172.
[2] J.V. Macpherson, A practical guide to using boron doped diamond in electrochemical research, Phys. Chem. Chem. Phys. 17 (2015) 2935–2949.
[3] K. Schwarzová-Pecková, J. Vosáhlová, J. Barek, I. Šloufová, E. Pavlova, V. Petrák, J. Zavázalová, Influence of boron content on the morphological, spectral, and electroanalytical characteristics of anodically oxidized boron-doped diamond electrodes, Electrochim. Acta 243 (2017) 170–182.
[4] L.A. Hutton, J.G. Iacobini, E. Bitziou, R.B. Channon, M.E. Newton, J.V. Macpherson, Examination of the factors affecting the electrochemical performance of oxygen-terminated polycrystalline boron-doped diamond electrodes, Anal. Chem. 85 (2013) 7230–7240.
[5] H.B. Suffredini, V.A. Pedrosa, L. Codognoto, S.A.S. Machado, R.C. Rocha-Filho, L.A. Avaca, Enhanced electrochemical response of boron-doped diamond electrodes brought on by a cathodic surface pre-treatment, Electrochim. Acta 49 (2004) 4021–4026.
[6] R.A. Medeiros, B.C. Lourencao, R.C. Rocha, O. Fatibello, Simultaneous voltammetric determination of synthetic colorants in food using a cathodically pretreated boron-doped diamond electrode, Talanta 97 (2012) 291–297.
[7] Y. Yardim, E. Keskin, Z. Senturk, Voltammetric determination of mixtures of caffeine and chlorogenic acid in beverage samples using a boron-doped diamond electrode, Talanta 116 (2013) 1010–1017.
[8] J. Barek, J. Fischer, T. Navratil, K. Peckova, B. Yosypchuk, J. Zima, Nontraditional electrode materials in environmental analysis of biologically active organic compounds, Electroanalysis 19 (2007) 2003–2014.
[9] J. Zavazalova, H. Dejmkova, J. Barek, K. Peckova, Voltammetric and amperometric determination of mixtures of aminobiphenyls and aminonaphthalenes using boron doped diamond electrode, Electroanalysis 25 (2013) 253–262.
[10] G.W. Muna, N. Tasheva, G.M. Swain, Electro-oxidation and amperometric detection of chlorinated phenols at boron-doped diamond electrodes: a comparison of microcrystalline and nanocrystalline thin films, Environ. Sci. Technol. 38 (2004) 3674–3682.
[11] J. Zavazalova, K. Prochazkova, K. Schwarzova-Peckova, Boron-doped diamond electrodes for voltammetric determination of benzophenone-3, Anal. Lett. 49 (2016) 80–91.
[12] R.F. Brocenschi, T.A. Silva, B.C. Lourencao, O. Fatibello, R.C. Rocha, Use of a boron-doped diamond electrode to assess the electrochemical response of the naphthol isomers and to attain their truly simultaneous electroanalytical determination, Electrochim. Acta 243 (2017) 374–381.
[13] I. Shpilevaya, J.S. Foord, Electrochemistry of methyl viologen and anthraquinone disulfonate at diamond and diamond powder electrodes: the influence of surface chemistry, Electroanalysis 26 (2014) 2088–2099.
[14] Y. Yardim, M. Gulcan, Z. Senturk, Determination of vanillin in commercial food product by adsorptive stripping voltammetry using a boron-doped diamond electrode, Food Chem. 141 (2013) 1821–1827.
[15] Y. Yardim, Electrochemical behavior of chlorogenic acid at a boron-doped diamond electrode and estimation of the antioxidant capacity in the coffee samples based on its oxidation peak, J. Food Sci. 77 (2012) C408–C413.
[16] H.S. Ali, A.A. Abdullah, P.T. Pinar, Y. Yardim, Z. Senturk, Simultaneous voltammetric determination of vanillin and caffeine in food products using an anodically pretreated boron-doped diamond electrode: its comparison with HPLC-DAD, Talanta 170 (2017) 384–391.
[17] A. Danhel, L. Havran, L. Trnkova, M. Fojta, Hydrogen evolution facilitates reduction of DNA guanine residues at the hanging mercury drop electrode: evidence for a chemical mechanism, Electroanalysis 28 (2016) 2785–2790.
[18] S.C.B. Oliveira, A.M. Oliveira-Brett, Boron doped diamond electrode pre-treatments effect on the electrochemical oxidation of dsDNA, DNA bases, nucleotides, homopolynucleotides and biomarker 8-oxoguanine, J. Electroanal. Chem. 648 (2010) 60–66.
[19] C. Prado, G.U. Flechsig, P. Grundler, J.S. Foord, F. Marken, R.G. Compton, Electrochemical analysis of nucleic acids at boron-doped diamond electrodes, Analyst 127 (2002) 329–332.
[20] A. Apilux, M. Tabata, O. Chailapakul, Electrochemical behaviors of native and thermally denatured fish DNA in the presence of cytosine derivatives and porphyrin by cyclic voltammetry using boron-doped diamond electrode, Bioelectrochemistry 70 (2007) 435–439.
[21] T.A. Ivandini, K. Honda, T.N. Rao, A. Fujishima, Y. Einaga, Simultaneous detection of purine and pyrimidine at highly boron-doped diamond electrodes by using liquid chromatography, Talanta 71 (2007) 648–655.
[22] L. Svorc, K. Kalcher, Modification-free electrochemical approach for sensitive monitoring of purine DNA bases: simultaneous determination of guanine and adenine in biological samples using boron-doped diamond electrode, Sensors Actuators B Chem. 194 (2014) 332–342.
[23] E. Fortin, J. Chane-Tune, D. Delabouglise, P. Bouvier, T. Livache, P. Mailley, B. Marcus, M. Mermoux, J.P. Petit, S. Szunerits, E. Vieil, Interfacing boron doped diamond and biology: an insight on its use for bioanalytical applications, Electroanalysis 17 (2005) 517–526.
[24] E. Fortin, E. Vieil, P. Mailley, S. Szunerits, T. Livache, Experimental and theoretical investigations on the adsorption of 2'-deoxyguanosine oxidation products at oxidized boron-doped diamond electrodes, Anal. Chem. 79 (2007) 3741–3746.
[25] E. Fortin, J. Chane-Tune, P. Mailley, S. Szunerits, B. Marcus, J.P. Petit, M. Mermoux, E. Vieil, Nucleosides and ODN electrochemical detection on to boron doped diamond electrodes, Bioelectrochemistry 63 (2004) 303–306.
[26] N. Yang, H. Uetsuka, E. Osawa, C.E. Nebel, Vertically aligned diamond nanowires for DNA sensing, Angew. Chem. Int. Ed. 47 (2008) 5183–5185.
[27] S. Hason, H. Pivonkova, V. Vetterl, M. Fojta, Label-free sequence-specific DNA sensing using copper-enhanced anodic stripping of purine bases at boron-doped diamond electrodes, Anal. Chem. 80 (2008) 2391–2399.
[28] J. Wang, G. Chen, A. Muck, D.C. Shin, A. Fujishima, Microchip capillary electrophoresis with a boron-doped diamond electrode for rapid separation and detection of purines, J. Chromatogr. A 1022 (2004) 207–212.
[29] N. Spataru, B.V. Sarada, D.A. Tryk, A. Fujishima, Anodic voltammetry of xanthine, theophylline, theobromine and caffeine at conductive diamond electrodes and its analytical application, Electroanalysis 14 (2002) 721–728.
[30] E. Palecek, M. Bartosik, Electrochemistry of nucleic acids, Chem. Rev. 112 (2012) 3427–3481.
[31] P. Subramanian, G. Dryhurst, Electrochemical oxidation of guanosine - formation of some novel guanine oligonucleosides, J. Electroanal. Chem. 224 (1987) 137–162.
[32] J. Spacek, A. Danhel, S. Hason, M. Fojta, Label-free detection of canonical DNA bases, uracil and 5-methylcytosine in DNA oligonucleotides using linear sweep voltammetry at a pyrolytic graphite electrode, Electrochem. Commun. 82 (2017) 34–38.
[33] P. Vidlakova, H. Pivonkova, M. Fojta, L. Havran, Electrochemical behavior of anthraquinone- and nitrophenyl-labeled deoxynucleoside triphosphates: a contribution to development of multipotential redox labeling of DNA, Monatsh. Chem. 146 (2015) 839–847.
[34] J. Balintova, M. Plucnara, P. Vidlakova, R. Pohl, L. Havran, M. Fojta, M. Hocek, Benzofurazane as a new redox label for electrochemical detection of DNA: towards multipotential redox coding of DNA bases, Chem. Eur. J. 19 (2013) 12720–12731.
[35] H. Cahova, L. Havran, P. Brazdilova, H. Pivonkova, R. Pohl, M. Fojta, M. Hocek, Aminophenyl- and nitrophenyl-labeled nucleoside triphosphates: synthesis, enzymatic incorporation, and electrochemical detection, Angew. Chem. Int. Ed. 47 (2008) 2059–2062.
[36] A. Danhel, Z. Trosanova, J. Balintova, L. Havran, M. Hocek, J. Barek, M. Fojta, Voltammetric analysis of 5-(4-Azidophenyl)-2'-deoxycytidine nucleoside and azidophenyl-labelled single- and double-stranded DNAs, Electrochim. Acta 215 (2016) 72–83.
[37] A. Danhel, Z. Trosanova, J. Balintova, A. Simonova, L. Pospisil, J. Cvacka, M. Hocek, M. Fojta, Electrochemical reduction of azidophenyl-deoxynucleoside conjugates at mercury surface, Electrochim. Acta 259 (2018) 377–385.
[38] A. Danhel, V. Raindlova, L. Havran, H. Pivonkova, M. Hocek, M. Fojta,

Electrochemical behaviour of 2,4-dinitrophenylhydrazi(o)ne as multi-redox centre DNA label at mercury meniscus modified silver solid amalgam electrode, Electrochim. Acta 126 (2014) 122–131.
[39] A. Daňhel, V. Raindlova, L. Havran, J. Barek, M. Hocek, M. Fojta, Voltammetric study of dsDNA modified by multi-redox label based on N-methyl-4-hydrazino-7-nitrobenzofurazan, Electrochim. Acta 129 (2014) 348–357.
[40] J. Musilova, J. Barek, K. Peckova, Determination of nitrophenols in drinking and river water by differential pulse voltammetry at boron-doped diamond film electrode, Electroanalysis 23 (2011) 1236–1244.
[41] G.S. Garbellini, G.R. Salazar-Banda, L.A. Avaca, Sonovoltammetric determination of 4-nitrophenol on diamond electrodes, J. Braz. Chem. Soc. 18 (2007) 1095–1099.
[42] V.A. Pedrosa, L. Codognoto, S.A.S. Machado, L.A. Avaca, Is the boron-doped diamond electrode a suitable substitute for mercury in pesticide analyses? A comparative study of 4-nitrophenol quantification in pure and natural waters, J. Electroanal. Chem. 573 (2004) 11–18.
[43] V.A. Pedrosa, H.B. Suffredini, L. Codognoto, S.T. Tanimoto, S.A.S. Machado, L.A. Avaca, Carbon surfaces for electroanalytical applications: a comparative study, Anal. Lett. 38 (2005) 1115–1125.
[44] V.D. Pedrosa, L. Codognoto, L.A. Avaca, Electroanalytical determination of 4-nitrophenol by square wave voltammetry on diamond electrodes, J. Braz. Chem. Soc. 14 (2003) 530–535.
[45] J. Karaova, J. Barek, K. Schwarzova-Peckova, Oxidative and reductive detection mode in determination of selected nitrophenols by HPLC with amperometric detection at boron doped diamond electrode, Anal. Lett. 49 (2016) 66–79.
[46] H. Dejmkova, J. Barek, J. Zima, Determination of aminonitrophenols in hair dyes using a carbon paste electrode and a boron-doped diamond film electrode - a comparative study, Int. J. Electrochem. Sci. 6 (2011) 3550–3563.
[47] M.S.D. Juliao, E.I. Ferreira, N.G. Ferreira, S.H.P. Serrano, Voltammetric detection of the interactions between RNO2 circle- and electron acceptors in aqueous medium at highly boron doped diamond electrode (HBDDE), Electrochim. Acta 51 (2006) 5080–5086.
[48] S. Chuanuwatanakul, O. Chailapakul, S. Motomizu, Electrochemical analysis of chloramphenicol using boron-doped diamond electrode applied to a flow-injection system, Anal. Sci. 24 (2008) 493–498.
[49] P. Samiec, T. Švorc, D.M. Stanković, M. Vojs, M. Marton, Z. Navrátilová, Mercury-free and modification-free electroanalytical approach towards bromazepam and alprazolam sensing: a facile and efficient assay for their quantification in pharmaceuticals using boron-doped diamond electrodes, Sensors Actuators B Chem. 245 (2017) 963–971.
[50] G.S. Garbellini, G.R. Salazar-Banda, L.A. Avaca, Sonovoltammetric determination of toxic compounds in vegetables and fruits using diamond electrodes, Food Chem. 116 (2009) 1029–1035.
[51] O. Yosypchuk, J. Barek, V. Vyskocil, Voltammetric determination of carcinogenic derivatives of pyrene using boron-doped diamond electrode, Anal. Lett. 45 (2012) 449–459.
[52] K. Cizek, J. Barek, J. Fischer, K. Peckova, J. Zima, Voltammetric determination of 3-nitrofluoranthene and 3-aminofluoranthene at boron doped diamond thin-film electrode, Electroanalysis 19 (2007) 1295–1299.
[53] J. Vosahlova, J. Zavazalova, V. Petrak, K. Schwarzova-Peckova, Factors influencing voltammetric reduction of 5-nitroquinoline at boron-doped diamond electrodes, Monatsh. Chem. 147 (2016) 21–29.
[54] J. Balintova, J. Spacek, R. Pohl, M. Brazdova, L. Havran, M. Fojta, M. Hocek, Azidophenyl as a click-transformable redox label of DNA suitable for electrochemical detection of DNA-protein interactions, Chem. Sci. 6 (2015) 575–587.
[55] K. Peckova, J. Barek, T. Navratil, B. Yosypchuk, J. Zima, Voltammetric determination of nitronaphthalenes at a silver solid amalgam electrode, Anal. Lett. 42 (2009) 2339–2363.
[56] E. Laviron, A. Vallat, R. Meunier-Prest, The reduction-mechanism of aromatic nitrocompounds in aqueous-medium. 5. The reduction of nitrosobenzene between Ph-0.4 and Ph-13, J. Electroanal. Chem. 379 (1994) 427–435.
[57] W. Zhang, S.Y. Zhu, R. Luque, S. Han, L.Z. Hu, G.B. Xu, Recent development of carbon electrode materials and their bioanalytical and environmental applications, Chem. Soc. Rev. 45 (2016) 715–752.
[58] I. Jiranek, K. Peckova, Z. Kralova, J.C. Moreira, J. Barek, The use of silver solid amalgam electrode for voltammetric and amperometric determination of nitroquinolines, Electrochim. Acta 54 (2009) 1939–1947.
[59] S. Komorsky-Lovric, M. Lovric, Square-wave voltammetry of quasi-reversible surface redox reactions, J. Electroanal. Chem. 384 (1995) 115–122.

Prohlášení o autorství

1. Comparison of carbon-based electrodes for detection of cresols in voltammetry and HPLC with electrochemical detection
   Vosáhlová J., Sochr J., Baluchová S., Švorc L., Taylor A., Schwarzová-Pecková K., Electroanalysis 32 (**2020**), published on-line, DOI: 10.1002/elan202060103, IF 2,550 (2019)
   Míra spoluautorství: 60 %

2. Voltammetric and adsorption study of 4-nitrophenyl-triazole-labeled 2'-deoxycytidine and 7-deazaadenosine nucleosides at boron-doped diamond electrode
   Vosahlova, J., Kolacna L., Danhel A., Fisher J., Balintova J., Hocek M., Schwarzova-Peckova K., Fojta M., Journal of Electroanalytical Chemistry 821 – (**2018**) 111-120, DOI :10.1016/j.jelechem.2018.01.003, IF 3,519
   Míra spoluautorství: 70 %

Jako zástupce spoluautorů prohlašuji, že se Mgr. Jana Vosáhlová podílela na níže uvedených publikovaných pracích uvedenou měrou.

Praha, 13. červen 2020

……..
doc. RNDr. Karolina Schwarzová, Ph.D.